

Lattice kinetic scheme for the Navier-Stokes equations coupled with convection-diffusion equations

Liang Wang,^{1,2,3} Weifeng Zhao,⁴ and Xiao-Dong Wang^{1,2,3,*}

¹*State Key Laboratory of Alternate Electrical Power System with Renewable Energy Sources, North China Electric Power University, Beijing 102206, China*

²*Research Center of Engineering Thermophysics, North China Electric Power University, Beijing 102206, China*

³*Key Laboratory of Condition Monitoring and Control for Power Plant Equipment of Ministry of Education, North China Electric Power University, Beijing 102206, China*

⁴*Department of Applied Mathematics and Mechanics, University of Science and Technology Beijing, Beijing 100083, China*



(Received 5 May 2018; revised manuscript received 26 July 2018; published 18 September 2018)

In this paper, we target two basic issues residing in some modified lattice kinetic schemes for the Navier-Stokes (NS) equations coupled with convection-diffusion equations (CDEs). First, a lattice Boltzmann (LB) model motivated by the lattice kinetic scheme (LKS) is presented for the NS equations coupled with CDEs. Due to the nonequilibrium schemes for the gradient terms contained in the equilibria as well as the discrete source term, the collision process of the present model can be implemented locally in both time and space. The Chapman-Enskog analysis shows that the macroscopic equations can be correctly recovered from the present model without additional assumptions. Second, we prove that the present modified LKS model, though written in the Bhatnagar-Gross-Krook (BGK) form, has two relaxation rates essentially. Based on this theoretical result, the modified lattice kinetic schemes in the literature should not be grouped as the BGK model, and the better numerical stability is intrinsically attributed to the adjustment of their two relaxation rates. Several benchmark thermal flow problems are simulated to validate the present model and the local nonequilibrium schemes for the shear rate and temperature gradient. The accuracy of the present model as well as its better numerical stability compared with the BGK model are verified, which supports our theoretical results. In addition, we also demonstrate that the regularized LB (RLB) model has two relaxation times as the present LKS model.

DOI: [10.1103/PhysRevE.98.033308](https://doi.org/10.1103/PhysRevE.98.033308)

I. INTRODUCTION

In many scientific and industrial areas, the Navier-Stokes (NS) equations coupled with convection-diffusion equations (CDEs) are generally used to prescribe hydrodynamic flows accompanied with convection heat-mass transfer. Owing to the strong nonlinearity of the governing equations and with the development of computer science and computational technology, it has been extensive to model the solutions to these equations with numerical methods. As an efficient and attractive numerical approach, the lattice Boltzmann method (LBM) has been applied to simulate complex fluid flows and transfer processes in fluids [1–3]. Compared with traditional numerical methods based on the macroscopic continuum equations, the LBM is analytically evolved from the mesoscopic Boltzmann equation and has many prominent merits, such as simple algorithm, easy boundary treatment, and inherently parallelizable computational property. In the past years, the LBM has been also extended to solve various nonlinear partial differential equations, including reaction-diffusion equations [4], wave equations [5,6], etc.

There have been several collision models in the LBM, including the Bhatnagar-Gross-Krook (BGK) (also called single-relaxation-time, SRT) model [7,8], the two-relaxation-

time (TRT) model [9–11], the entropic model [12,13], the cascaded or central-moment-based model [14], the cumulant model [15], and the multiple-relaxation-time (MRT) model [16–18]. The difference between these models resides in the collision operators adopted in the LBE. Among these collision models, the BGK model, the TRT model, and the MRT model have been extensively applied to solve the NS equations coupled with convection-diffusion equations (CDEs) [9,11,19,20] till now. The BGK model is the simplest in appearance and thus is the most commonly used model. However, as pointed out in previous literature, there are some inherent deficiencies when using the BGK collision model [16,17,21]. The most well-known defect is the numerical instability at relatively small viscosity (high Reynolds number) and/or effective thermal diffusivity. In recent years, there are some efforts to overcome the shortcomings of BGK-based models by changing the equilibrium distribution function and/or modifying the BGK collision model [22]. For Darcy's flow in porous media, it is shown in Ref. [23] that the viscosity dependence of permeability [24] can be remedied if the dependence from the Knudsen number is additionally considered in the BGK model. The MRT model is the most general form developed from the generalized lattice Boltzmann equation (LBE) model [25]—it includes the maximum number of multiple relaxations to optimize the LBE. It has been indicated that the MRT models can provide significant improvements over their BGK counterparts in terms of accuracy and stability [16,17,19,24].

*Corresponding author: wangxd99@gmail.com

With the benefit from two most important relaxation rates in the LBE, the TRT model shares some advantages of the MRT model in terms of stability and accuracy, and remains simplicity and computational efficiency as the BGK model. From this point, the TRT model can be regarded as a bridge between the MRT model and the BGK model.

To reduce computer memory in simulating incompressible flows with heat transfer, a lattice kinetic scheme (LKS), coalescing the kinetic scheme with the LBM, was proposed in Ref. [26], where the relaxation time is set to be unity and thus the velocity distribution function is not needed. By incorporating the shear rate (or temperature gradient) into the equilibrium distribution function, the fluid viscosity (or thermal diffusivity) in the LKS can be determined by another parameter different from the relaxation time. This idea was subsequently extended to LB models for two-phase flows [27,28], non-Newtonian fluid flows [29], and thermal flows [30]. However, the mass conservation in the LKS is not strictly ensured, and in some LKS models [26–29] the shear rate (or temperature gradient) is computed by the finite difference scheme, which not only spoils the localization of collision process in the LBE but also brings about some difficulties to treat complex boundary conditions by a local scheme. Recently, this defect has been addressed in the modified LKS model for fluid flows [31,32]. In the modified model, the local mass conservation is guaranteed, and the nonequilibrium distribution function is employed to compute the shear rate rather than by the nonlocal finite-difference scheme. For solving the NS equations and CDE, similar modifications have also been made within the BGK framework [32] and later generalized to the MRT version [33]. It is shown in Refs. [26,31–33] that the LKS and its modified versions can improve numerical stability at low viscosity and thermal diffusivity. Realizing this benefit, the LKS has been further modified and extended from pure fluid flows to flow and heat transfer in porous media at the representative elementary volume (REV) scale [34], axisymmetric thermal flows [35], and flow and mass transfer in porous media at the REV scale [36].

In all the above works on modifications of LKS as well as some following cited papers [37–39], it was claimed that the modified LKS model is a BGK model since the collision operator is expressed in the BGK framework. The better numerical stability than the standard BGK model is attributed to an additional parameter introduced to make the dimensionless relaxation time adjustable. However, Inamuro [26] pointed out that the extra parameter in the LKS model may be regarded as a relaxation parameter linked to the stress tensor. This indicates that the LKS model could not be considered as a BGK model. Thus, these two different perspectives bring about an essential question whether the LKS and its modified models are the BGK model. Recently, as for the NS equations, we show in Ref. [40] that the modified LKS model [31] is a LB model with two relaxation times. However, it is unresolved till now whether the modified LKS model for the CDE coupled with the NS equations also has two relaxation times.

Hence, the present work aims to fulfill a theoretical proof that ascertains the essence of collision operators in the modified LKS model for the NS equations coupled with CDEs. For the modified LKS models to solve the two equations, we note that through the Chapman-Enskog analysis the CDE without

the source term can be recovered with a deviation term in Ref. [32]. Although this deviation term can be neglected under some assumptions (e.g., constant velocity or the low Mach number assumption), it still has an influence on the accuracy of the LB model [41]. The unwanted deviation term in the recovered CDE disappears with the assumption of low Mach number in Ref. [33], however, the included time-derivative terms in the evolution equation spoil the locality of collision process in time. Therefore, a new modified LKS model, which cannot only satisfy the consistency of recovered equations with the macroscopic equations with the source term but also guarantee the localization of collision process in time and space, is first presented for the NS equations coupled with CDEs. Also, the shear rate and temperature gradient are locally calculated by the nonequilibrium schemes. The modified LKS provides two additional parameters besides the relaxation time for the fluid viscosity and diffusion coefficient. With the local scheme for the gradient term, the evolution equation of the modified LKS model is then rewritten in vector form to retract the collision matrix. To diagonalize the collision matrices in the generalized LBEs, this work designs a new transformation matrix different from that in Ref. [40]. According to the eigenvalues of the diagonalized collision matrices, the modified LKS for the NS equations coupled with CDEs is proved to have two relaxation rates, which accounts for the better numerical stability of the modified LKS model than the standard BGK model. Additionally, the diagonalization process is also performed on the regularized LB (RLB) model [42,43] to determine the relaxation rates in the collision matrix. Finally, the presented LKS model and its better numerical stability is validated by some numerical experiments.

The paper is organized as follows. In Sec. II, the modified LKS model, as well as a local scheme for the gradient terms, is presented for the NS equations and CDEs. Section III is devoted to our theoretical proof that the modified LKS model as well as the RLB model essentially has two relaxation rates. In Sec. IV, some numerical examples are performed to validate the modified LKS model and test its numerical stability. The paper is closed by a brief conclusion in Sec. V.

II. LATTICE BOLTZMANN MODEL FOR THE NS EQUATIONS COUPLED WITH CDES

In this section, a LB model based on the LKS is presented for the NS equations coupled with CDEs. The model adopts the double distribution function approach: the LBE of density distribution function for the NS equations and the LBE of scalar (temperature or concentration) distribution function for the CDE. For the involved spatial gradient terms, a local computing scheme, instead of the nonlocal finite-difference-scheme, is provided.

A. Macroscopic equations

The standard macroscopic equations considered here are expressed as follows:

$$\partial_t \rho + \nabla \cdot (\rho \mathbf{u}) = 0, \quad (1a)$$

$$\partial_t (\rho \mathbf{u}) + \nabla \cdot (\rho \mathbf{u} \mathbf{u}) = -\nabla p + \nabla \cdot \boldsymbol{\tau} + \rho \mathbf{a}, \quad (1b)$$

$$\partial_t \phi + \nabla \cdot (\mathbf{u} \phi) = \nabla \cdot (D \nabla \phi) + Q, \quad (2)$$

where ρ , \mathbf{u} , and p are the density, velocity, and pressure of fluid, ϕ is a scalar variable (e.g., temperature, concentration, etc.), \mathbf{a} denotes the acceleration due to external forces, D is the diffusion coefficient, and Q is the source term. Here, $\boldsymbol{\tau}$ is a second-order tensor standing for the shear stress and defined by $\boldsymbol{\tau} = \rho\nu\mathbf{S}$, where ν is the kinematic viscosity of fluid, and \mathbf{S} is the shear rate defined as

$$\mathbf{S} = \nabla\mathbf{u} + (\nabla\mathbf{u})^T, \quad (3)$$

where the superscript T denotes the transposition operator.

B. Model description

As noted in the Introduction, there are some improvements needed in previous modified LKS models for Eqs. (1) and (2) [32,33]. To this end and inspired by the idea of Chai and Zhao [44], we base on some recent works about modified LKS [31,32,34] to present a new LB model for Eqs. (1) and (2). Same as the original LKS [26], our model is written in the form of BGK model first. In the BGK framework, we would note that the Chapman-Enskog analysis on the present model to recover the macroscopic equations is like those in Refs. [31,32,34] and thus is not presented in this subsection.

For the NS equations in Eq. (1), the evolution equation is expressed as

$$f_i(\mathbf{x} + \mathbf{c}_i\delta_t, t + \delta_t) - f_i(\mathbf{x}, t) = -\frac{1}{\tau_f}[f_i(\mathbf{x}, t) - \tilde{f}_i^{(\text{eq})}(\mathbf{x}, t)] + \delta_t F_i(\mathbf{x}, t), \quad (4)$$

where $f_i(\mathbf{x}, t)$ is the distribution function corresponding to the discrete velocity \mathbf{c}_i at time t and position \mathbf{x} , δ_t is the time

increment, τ_f is the dimensionless relaxation time, $\tilde{f}_i^{(\text{eq})}(\mathbf{x}, t)$ is the equilibrium distribution function, and F_i is the external force term.

On the basis of LKS model, the equilibrium distribution function (EDF) is constructed by including the shear rate and is defined by

$$\tilde{f}_i^{(\text{eq})}(\mathbf{x}, t) = \omega_i \rho \left[1 + \frac{\mathbf{c}_i \cdot \mathbf{u}}{c_s^2} + \frac{\mathbf{u}\mathbf{u} : (\mathbf{c}_i \mathbf{c}_i - c_s^2 \mathbf{I})}{2c_s^4} \right] + \omega_i \rho \frac{A\delta_t \mathbf{S} : (\mathbf{c}_i \mathbf{c}_i - c_s^2 \mathbf{I})}{2c_s^2}, \quad (5)$$

where ω_i are the weight coefficients, c_s is the sound speed, \mathbf{I} is the identity tensor, and A is an additional parameter combined with τ_f to determine the fluid viscosity. To avoid the discrete effect in the recovered macroscopic equations, the forcing term is taken as [45]

$$F_i = \omega_i \rho \left(1 - \frac{1}{2\tau_f} \right) \left[\frac{\mathbf{c}_i \cdot \mathbf{a}}{c_s^2} + \frac{(\mathbf{u}\mathbf{a} + \mathbf{a}\mathbf{u}) : (\mathbf{c}_i \mathbf{c}_i - c_s^2 \mathbf{I})}{2c_s^4} \right]. \quad (6)$$

The fluid density ρ and velocity \mathbf{u} are computed by the distribution function

$$\rho = \sum_i f_i, \quad \rho\mathbf{u} = \sum_i \mathbf{c}_i f_i + \frac{\delta_t}{2} \rho \mathbf{a}. \quad (7)$$

For the two-dimensional dimension case, the discrete velocity \mathbf{c}_i adopts the D2Q9 model, which is given by

$$\mathbf{c}_i = \begin{cases} c(0, 0), & i = 0, \\ c(\cos[(i-1)\pi/2], \sin[(i-1)\pi/2]), & i = 1-4, \\ 2c(\cos[(i-1)\pi/2 + \pi/4], \sin[(i-1)\pi/2 + \pi/4]), & i = 5-8, \end{cases} \quad (8)$$

where $c = \delta x / \delta t$ is the lattice speed, and δ_x is the lattice spacing. Correspondingly, the above sound speed $c_s = c/\sqrt{3}$, and the weight coefficients are given by $\omega_0 = 4/9$, $\omega_{1-4} = 1/9$ and $\omega_{5-8} = 1/36$. Through the Chapman-Enskog analysis (see Refs. [31,32,34] and reference therein), the NS Eqs. (1) can be correctly recovered from the LBE (5) and the shear viscosity is given by

$$\nu = c_s^2 (\tau_f - A - \frac{1}{2}) \delta_t. \quad (9)$$

For the CDE (2) in which the velocity \mathbf{u} obeys the NS Eqs. (1), the evolution equation of the present model is written as

$$g_i(\mathbf{x} + \mathbf{c}_i\delta_t, t + \delta_t) - g_i(\mathbf{x}, t) = -\frac{1}{\tau_\phi}[g_i(\mathbf{x}, t) - \tilde{g}_i^{(\text{eq})}(\mathbf{x}, t)] + \delta_t G_i(\mathbf{x}, t), \quad (10)$$

where g_i and $\tilde{g}_i^{(\text{eq})}$ are the distribution function and its equilibrium associated with the scalar ϕ , τ_ϕ is the relaxation time, and G_i is the source term. Similar to Eq. (5), the above $\tilde{g}_i^{(\text{eq})}$ contains an additional parameter B with the spatial gradient

and is given by

$$\tilde{g}_i^{(\text{eq})} = \omega_i \phi \left[1 + \frac{\mathbf{c}_i \cdot \mathbf{u}}{c_s^2} + \frac{\mathbf{u}\mathbf{u} : (\mathbf{c}_i \mathbf{c}_i - c_s^2 \mathbf{I})}{2c_s^4} \right] + \varpi_i \phi + \omega_i B \delta_t \mathbf{c}_i \cdot \nabla \phi, \quad (11)$$

and G_i is

$$G_i = \omega_i \left(1 - \frac{1}{2\tau_\phi} \right) \left[\frac{\mathbf{c}_i \cdot (\phi \mathbf{a} + c_s^2 \nabla \phi)}{c_s^2} + \left(1 + \frac{\mathbf{c}_i \cdot \mathbf{u}}{c_s^2} \right) Q \right], \quad (12)$$

where the coefficient ϖ_i is related with ω_i as $\varpi_0 = \omega_0 - 1 = -5/9$, $\varpi_i = \omega_i (i \neq 0)$.

The scalar variable ϕ is computed by

$$\phi = \sum_i g_i + \frac{\delta_t}{2} Q. \quad (13)$$

Following the multiscale expansion procedure presented in Refs. [31,32,34], the CDE (2) can be recovered from the above

model and the diffusion coefficient D is computed as

$$D = c_s^2(\tau_\phi - B - \frac{1}{2})\delta_t. \quad (14)$$

Furthermore, to ensure the locality of collision process, the appeared space derivatives in the present model, i.e., \mathbf{S} and $\nabla\phi$ should be calculated locally. Actually, these two terms can be computed from the nonequilibrium part of the distribution function with second-order convergence rate [31,34,44], which are given by

$$\begin{aligned} \mathbf{S} &= \frac{\sum_i \mathbf{c}_i \mathbf{c}_i [f_i - f_i^{(\text{eq})}] + \frac{\delta_t}{2} \rho(\mathbf{u}\mathbf{a} + \mathbf{a}\mathbf{u})}{c_s^2 \rho (A - \tau_f) \delta_t}, \\ \nabla\phi &= \frac{\sum_i \mathbf{c}_i [g_i - g_i^{(\text{eq})}] + \frac{\delta_t}{2} (\phi\mathbf{a} + \mathbf{u}Q)}{c_s^2 (B - \tau_\phi - \frac{1}{2}) \delta_t}, \end{aligned} \quad (15)$$

where $f_i^{(\text{eq})}$ and $g_i^{(\text{eq})}$ are parts of the EDF Eqs. (5) and (11) and defined as

$$\begin{aligned} f_i^{(\text{eq})}(\mathbf{x}, t) &= \omega_i \rho \left[1 + \frac{\mathbf{c}_i \cdot \mathbf{u}}{c_s^2} + \frac{\mathbf{u}\mathbf{u} : (\mathbf{c}_i \mathbf{c}_i - c_s^2 \mathbf{I})}{2c_s^4} \right], \\ g_i^{(\text{eq})} &= \omega_i \phi \left[1 + \frac{\mathbf{c}_i \cdot \mathbf{u}}{c_s^2} + \frac{\mathbf{u}\mathbf{u} : (\mathbf{c}_i \mathbf{c}_i - c_s^2 \mathbf{I})}{2c_s^4} \right] + \varpi_i \phi. \end{aligned} \quad (16)$$

As can be seen, the evolution equations of the present modified LKS model can be implemented locally in time and space. From the Chapman-Enskog analysis (as will shown in Appendix B), the NS Eqs. (1) and the CDE (2) can be recovered correctly from the present model without any approximations. Two additional parameters A and B are introduced with the relaxation times to compute the fluid viscosity and diffusion coefficient. As $A = 0$ and $B = 0$, one can see that the present model will become the standard BGK version as proposed in Ref. [44]. This indicates that the present modified LKS model can possess superior numerical stability than the BGK model. In the subsequent section, we will prove that the better numerical stability of the present modified model is essentially due to the essence that it has two relaxation rates.

III. ESSENCE OF THE COLLISION OPERATOR

This section shows that the presented LKS model for the NS Eqs. (1) and the CDE (2) actually have two relaxation rates

as the TRT model. To prove this, the key task is to determine the eigenvalue of collision matrices in the generalized LBE of the present model. In the following, the theoretical proof is provided and some primary results are presented in the Appendix.

As a first step, we substitute the terms of \mathbf{S} and $\nabla\phi$ given by Eq. (16) into Eqs. (4) and (10), and the following vector equations of post-collision distributions can be obtained

$$\begin{aligned} \mathbf{f}^{\text{post}} &= \mathbf{f} - \frac{1}{\tau_f} [\mathbf{f} - \mathbf{f}^{(\text{eq})}] \\ &\quad + \frac{A}{\tau_f (A - \tau_f)} \mathbf{D} [\mathbf{f} - \mathbf{f}^{(\text{eq})}] + \delta_t \hat{\mathbf{F}}, \end{aligned} \quad (17)$$

$$\begin{aligned} \mathbf{g}^{\text{post}} &= \mathbf{g} - \frac{1}{\tau_\phi} [\mathbf{g} - \mathbf{g}^{(\text{eq})}] \\ &\quad + \frac{B + \tau_\phi - \frac{1}{2}}{\tau_\phi (B - \tau_\phi - \frac{1}{2})} \mathbf{R} [\mathbf{g} - \mathbf{g}^{(\text{eq})}] + \delta_t \hat{\mathbf{G}}, \end{aligned} \quad (18)$$

where $\mathbf{f} = (f_0(\mathbf{x}, t), f_1(\mathbf{x}, t), \dots, f_8(\mathbf{x}, t))^T$ and $\mathbf{g} = (g_0(\mathbf{x}, t), g_1(\mathbf{x}, t), \dots, g_8(\mathbf{x}, t))^T$ are 9-dimensional vectors of the discrete distribution functions $f_i(\mathbf{x}, t)$ and $g_i(\mathbf{x}, t)$; $\mathbf{f}^{(\text{eq})}$ and $\mathbf{g}^{(\text{eq})}$ are 9-dimensional vectors consist of $f_i^{(\text{eq})}$ and $g_i^{(\text{eq})}$ defined by Eq. (16); $\hat{\mathbf{F}}$ and $\hat{\mathbf{G}}$ are two column vectors of some discrete terms which are respectively expressed as

$$\begin{aligned} \hat{F}_i &= \omega_i \rho \left(1 - \frac{1}{2\tau_f} \right) \frac{\mathbf{c}_i \cdot \mathbf{a}}{c_s^2} + \omega_i \rho \left[1 + \frac{1}{2(A - \tau_f)} \right] \\ &\quad \times \frac{(\mathbf{u}\mathbf{a} + \mathbf{a}\mathbf{u}) : (\mathbf{c}_i \mathbf{c}_i - c_s^2 \mathbf{I})}{2c_s^4}, \end{aligned} \quad (19)$$

$$\begin{aligned} \hat{G}_i &= \omega_i \left(1 - \frac{1}{2\tau_\phi} \right) \left[\left(1 + \frac{\mathbf{c}_i \cdot \mathbf{u}}{c_s^2} \right) Q + \frac{\mathbf{c}_i \cdot \mathbf{a}}{c_s^2} \rho \phi \right] \\ &\quad + \omega_i \frac{1}{2\tau_\phi} \frac{B + \tau_\phi - \frac{1}{2}}{B - \tau_\phi - \frac{1}{2}} \frac{\mathbf{c}_i \cdot (\rho \mathbf{a} \phi + \mathbf{u}Q)}{c_s^2}, \end{aligned} \quad (20)$$

\mathbf{D} and \mathbf{R} are two 9×9 linear matrices and given by

$$D_{i,j} = \omega_i \frac{1}{2c_s^4} [\mathbf{c}_j \mathbf{c}_j : (\mathbf{c}_i \mathbf{c}_i - c_s^2 \mathbf{I})], \quad R_{i,j} = \omega_i \frac{1}{c_s^2} \mathbf{c}_i \cdot \mathbf{c}_j. \quad (21)$$

The explicit forms of matrices \mathbf{D} and \mathbf{R} are written as

$$\mathbf{D} = \frac{1}{12} \begin{pmatrix} 0 & -8 & -8 & -8 & -8 & -16 & -16 & -16 & -16 \\ 0 & 4 & -2 & 4 & -2 & 2 & 2 & 2 & 2 \\ 0 & -2 & 4 & -2 & 4 & 2 & 2 & 2 & 2 \\ 0 & 4 & -2 & 4 & -2 & 2 & 2 & 2 & 2 \\ 0 & -2 & 4 & -2 & 4 & 2 & 2 & 2 & 2 \\ 0 & 1 & 1 & 1 & 1 & 5 & -1 & 5 & -1 \\ 0 & 1 & 1 & 1 & 1 & -1 & 5 & -1 & 5 \\ 0 & 1 & 1 & 1 & 1 & 5 & -1 & 5 & -1 \\ 0 & 1 & 1 & 1 & 1 & -1 & 5 & -1 & 5 \end{pmatrix}, \quad (22)$$

$$\mathbf{R} = \frac{1}{12} \begin{pmatrix} 0 & 0 & 0 & 0 & 0 & 0 & 0 & 0 & 0 \\ 0 & 4 & 0 & -4 & 0 & 4 & -4 & -4 & 4 \\ 0 & 0 & 4 & 0 & -4 & 4 & 4 & -4 & -4 \\ 0 & -4 & 0 & 4 & 0 & -4 & 4 & 4 & -4 \\ 0 & 0 & -4 & 0 & 4 & -4 & -4 & 4 & 4 \\ 0 & 1 & 1 & -1 & -1 & 2 & 0 & -2 & 0 \\ 0 & -1 & 1 & 1 & -1 & 0 & 2 & 0 & -2 \\ 0 & -1 & -1 & 1 & 1 & -2 & 0 & 2 & 0 \\ 0 & 1 & -1 & -1 & 1 & 0 & -2 & 0 & 2 \end{pmatrix}. \quad (23)$$

From Eqs. (17) and (18), one can see that the collision matrices in the generalized LBEs of f and g are, respectively, as follows:

$$\Lambda_f = \frac{1}{\tau_f} \mathbf{I} - \frac{A}{\tau_f(A - \tau_f)} \mathbf{D}, \quad \Lambda_g = \frac{1}{\tau_\phi} \mathbf{I} - \frac{B + \tau_\phi - \frac{1}{2}}{\tau_\phi(B - \tau_\phi - \frac{1}{2})} \mathbf{R}. \quad (24)$$

Through some mathematical manipulations, we can deduce that $\mathbf{D}^2 = \mathbf{D}$ and $\mathbf{R}^2 = \mathbf{R}$ together with the traces $\text{tr}(\mathbf{D}) = 3$, $\text{tr}(\mathbf{R}) = 2$ (see Appendix A for details). Mathematically, these results indicate that the matrices \mathbf{D} and \mathbf{R} can be diagonalized to a diagonal one with entries of 0 or 1, and there are three and two entries of 1 respectively in the diagonalized matrix of \mathbf{D} and \mathbf{R} .

Next, special attention is paid to diagonalize \mathbf{D} and \mathbf{R} . In our previous paper focusing on the stability analysis of some lattice kinetic schemes for NS equations [40], an invertible matrix, which is a variant of the transformation matrix \mathbf{M} in the MRT model [17], was provided to diagonalize the matrix \mathbf{D} . However, we point out that this invertible matrix cannot diagonalize the matrix \mathbf{R} in the present modified LKS model for CDE. A different matrix should be searched to diagonalize \mathbf{R} . Note that the D2Q9 discrete velocity model is adopted for both the NS equations and CDE in the present model. Therefore, to obtain the *common* invertible matrix to simultaneously diagonalize \mathbf{D} and \mathbf{R} , we still refer to the widely used matrix \mathbf{M} [17] to construct an invertible matrix \mathbf{T} as

$$\mathbf{T} = \begin{pmatrix} 1 & 1 & 1 & 1 & 1 & 1 & 1 & 1 & 1 \\ 0 & 3 & 3 & 3 & 3 & 6 & 6 & 6 & 6 \\ 0 & -3 & -3 & -3 & -3 & 3 & 3 & 3 & 3 \\ 0 & 1 & 0 & -1 & 0 & 1 & -1 & -1 & 1 \\ 0 & -1 & 0 & 1 & 0 & 2 & -2 & -2 & 2 \\ 0 & 0 & 1 & 0 & -1 & 1 & 1 & -1 & -1 \\ 0 & 0 & -1 & 0 & 1 & 2 & 2 & -2 & -2 \\ 0 & 1 & -1 & 1 & -1 & 0 & 0 & 0 & 0 \\ 0 & 0 & 0 & 0 & 0 & 1 & -1 & 1 & -1 \end{pmatrix}. \quad (25)$$

Here, \mathbf{T} relates to the matrix \mathbf{M} via the following elementary transformation:

$$\mathbf{T} = \mathbf{U}\mathbf{M}, \quad (26)$$

where

$$\mathbf{U} = \begin{pmatrix} 1 & 0 & 0 & 0 & 0 & 0 & 0 & 0 & 0 \\ 4 & 1 & 0 & 0 & 0 & 0 & 0 & 0 & 0 \\ 0 & 1 & 1 & 0 & 0 & 0 & 0 & 0 & 0 \\ 0 & 0 & 0 & 1 & 0 & 0 & 0 & 0 & 0 \\ 0 & 0 & 0 & 1 & 1 & 0 & 0 & 0 & 0 \\ 0 & 0 & 0 & 0 & 0 & 1 & 0 & 0 & 0 \\ 0 & 0 & 0 & 0 & 0 & 1 & 1 & 0 & 0 \\ 0 & 0 & 0 & 0 & 0 & 0 & 0 & 1 & 0 \\ 0 & 0 & 0 & 0 & 0 & 0 & 0 & 0 & 1 \end{pmatrix}, \quad \mathbf{M} = \begin{pmatrix} 1 & 1 & 1 & 1 & 1 & 1 & 1 & 1 & 1 \\ -4 & -1 & -1 & -1 & -1 & 2 & 2 & 2 & 2 \\ 4 & -2 & -2 & -2 & -2 & 1 & 1 & 1 & 1 \\ 0 & 1 & 0 & -1 & 0 & 1 & -1 & -1 & 1 \\ 0 & -2 & 0 & 2 & 0 & 1 & -1 & -1 & 1 \\ 0 & 0 & 1 & 0 & -1 & 1 & 1 & -1 & -1 \\ 0 & 0 & -2 & 0 & 2 & 1 & 1 & -1 & -1 \\ 0 & 1 & -1 & 1 & -1 & 0 & 0 & 0 & 0 \\ 0 & 0 & 0 & 0 & 0 & 1 & -1 & 1 & -1 \end{pmatrix}. \quad (27)$$

With the matrix \mathbf{T} , one can directly verify that

$$\begin{aligned} \mathbf{T}\mathbf{D}\mathbf{T}^{-1} &= \mathbf{S}_D = \text{diag}(0, 1, 0, 0, 0, 0, 0, 1, 1), \\ \mathbf{T}\mathbf{R}\mathbf{T}^{-1} &= \mathbf{S}_R = \text{diag}(0, 0, 0, 1, 0, 1, 0, 0, 0). \end{aligned} \quad (28)$$

Hence, the vector Eqs. (17) and (18) can be further rewritten as

$$\begin{aligned} \mathbf{f}^{\text{post}} &= \mathbf{f} - \mathbf{T}^{-1} \mathbf{S}_f \mathbf{T} [\mathbf{f} - \mathbf{f}^{(\text{eq})}] + \delta_t \hat{\mathbf{F}}, \\ \mathbf{g}^{\text{post}} &= \mathbf{g} - \mathbf{T}^{-1} \mathbf{S}_g \mathbf{T} [\mathbf{g} - \mathbf{g}^{(\text{eq})}] + \delta_t \hat{\mathbf{G}}, \end{aligned} \quad (29)$$

where S_f and S_g are given by

$$S_f = \frac{1}{\tau_f} \mathbf{I} - \frac{A}{\tau_f(A - \tau_f)} S_D = \text{diag} \left(\frac{1}{\tau_f}, \frac{1}{\tau_f - A}, \frac{1}{\tau_f}, \frac{1}{\tau_f}, \frac{1}{\tau_f}, \frac{1}{\tau_f}, \frac{1}{\tau_f}, \frac{1}{\tau_f - A}, \frac{1}{\tau_f - A} \right), \quad (30)$$

$$S_g = \frac{1}{\tau_\phi} \mathbf{I} - \frac{B + \tau_\phi - \frac{1}{2}}{\tau_\phi(B - \tau_\phi - \frac{1}{2})} S_R = \text{diag} \left(\frac{1}{\tau_\phi}, \frac{1}{\tau_\phi}, \frac{1}{\tau_\phi}, \frac{2}{\tau_\phi - B + \frac{1}{2}}, \frac{1}{\tau_\phi}, \frac{2}{\tau_\phi - B + \frac{1}{2}}, \frac{1}{\tau_\phi}, \frac{1}{\tau_\phi}, \frac{1}{\tau_\phi} \right). \quad (31)$$

Clearly, there are two eigenvalues, that is, $\{\frac{1}{\tau_f}, \frac{1}{\tau_f - A}\}$ and $\{\frac{1}{\tau_\phi}, \frac{2}{\tau_\phi - B + \frac{1}{2}}\}$, respectively, for the matrices S_f and S_g . These results show us that the present modified model Eqs. (4) and (10) essentially has two relaxation rates, respectively, given by $\{\frac{1}{\tau_f}, \frac{1}{\tau_f - A}\}$ and $\{\frac{1}{\tau_\phi}, \frac{2}{\tau_\phi - B + \frac{1}{2}}\}$.

The above proof definitely shows that the present LKS model has two relaxation rates as the TRT model. However, there are some principle differences between these two models. For the TRT model of Ginzburg *et al.* in Refs. [10,11], the collisions of populations are decomposed into the symmetric and antisymmetric parts, and the two relaxation parameters correspond to and determine the evolution of the symmetric and antisymmetric collision components. In this way, the accuracy and stability can be improved by adjusting the symmetric and antisymmetric relaxation parameters. While, the two relaxation rates in the present LKS model are only associated with the evolution of symmetrical collision part. The numerical stability is improved by adjusting the additional parameter besides the relaxation time to compute the viscosity. In addition, as revealed in Refs. [10,19], when the eigenvalues, associated with the even- and odd-order polynomial MRT-basis vectors, are set to the symmetric and antisymmetric relaxation rates, the TRT model can be derived from the MRT model. Via the transform matrix \mathbf{M} , the diagonalized collision matrix of the TRT model is $S_f = \text{diag}(s_v, s_v, s_v, s_q, s_q, s_q, s_q, s_v, s_v)$, where s_v corresponds to the even-order nonconserved moments, while s_q corresponds to the odd-order ones. For the present modified LKS, we note that the matrix \mathbf{M} cannot be used to diagonalize the collision matrix, and additionally the corresponding S_f given by Eq. (30) is different from that in the Ginzburg TRT model even as $s_v = \frac{1}{\tau_f - A}$, $s_q = \frac{1}{\tau_f}$. This indicates that the relaxation rates here do not strictly correspond to the even- and odd-order nonconserved moments. Based on these reasons, the present LKS model cannot be categorized into the TRT model.

It is shown in Refs. [46,47] that the so-called M10 model has two relaxation rates corresponding to even-order nonconserved moments but is essentially not a TRT model as the present LKS model. However, there are several differences between the LKS model and the M10 model. For the M10 model [46,47], two different relaxation rates, corresponding to second-order nonconserved moments, are employed respectively for the shear and bulk viscosities, and the other relaxation rates for odd-order and fourth-order nonconserved moments are all set to unity. However, the two viscosities in the present LKS model have the same value, because the corresponding relaxation rates are both $\frac{1}{\tau_f - A}$, and the remaining relaxation rates are taken to be $\frac{1}{\tau_f}$ but not unity. In addition, the eigenvectors of collision operator for the M10

model form a matrix with weighted orthogonal rows, while the transformation matrix in the present LKS model does not satisfy the orthogonality property.

Since a LB model developed from the LKS is written in the SRT form, it is usually regarded as a modified BGK model in previous literature. As noted above, the better numerical stability is attributed to the additional parameter introduced with the relaxation time to determine the fluid viscosity and diffusion coefficient. However, from the above proof in this work, the better numerical stability of modified LKS models for the NS equations coupled with CDEs should be due to an enhanced degree of freedom from their two relaxation rates. Now, some remarks from the above results are presented below.

Remark 1. In diagonalizing \mathbf{D} to the matrix S_D , the present invertible matrix \mathbf{T} is different from that in Ref. [40] (reference therein). This indicates that the transformation matrix for the present LKS model is not unique, and other transformation matrix can be also found by remoulding the widely used matrix \mathbf{M} in Ref. [17].

Remark 2. The computing schemes Eq. (15) for \mathbf{S} and $\nabla\phi$ are derived from the Chapman-Enskog analysis on Eqs. (4) and (10) within the framework of BGK model. While along with the MRT framework, the Chapman-Enskog analysis on the present LKS model provides the computations of \mathbf{S} and $\nabla\phi$ in moment space (see Appendix B for details)

$$\begin{aligned} \partial_x u_x + \partial_y u_y &= -\frac{m_1 - m_1^{(0)} + 3\delta_t \rho \mathbf{a} \cdot \mathbf{u}}{2\rho(\tau_f - A)\delta_t}, \\ \partial_x u_x - \partial_y u_y &= -\frac{3[m_7 - m_7^{(0)} + \delta_t \rho(a_x u_x - a_y u_y)]}{2\rho(\tau_f - A)\delta_t}, \\ \partial_x u_y + \partial_y u_x &= -\frac{3[m_8 - m_8^{(0)} + \frac{1}{2}\delta_t \rho(a_y u_x + a_x u_y)]}{\rho(\tau_f - A)\delta_t}, \end{aligned} \quad (32)$$

and

$$\begin{aligned} \partial_x \phi &= -\frac{3}{2\delta_t} \frac{2[q_3 - q_3^{(0)}] + \delta_t(\phi a_x + u_x Q)}{\tau_\phi - B + \frac{1}{2}}, \\ \partial_y \phi &= -\frac{3}{2\delta_t} \frac{2[q_5 - q_5^{(0)}] + \delta_t(\phi a_y + u_y Q)}{\tau_\phi - B + \frac{1}{2}}, \end{aligned} \quad (33)$$

where $\mathbf{u} = (u_x, u_y)$ and $\mathbf{a} = (a_x, a_y)$, $m_{1,7,8}$ and $q_{3,5}$ are certain elements of transformed moments respectively from \mathbf{f} and \mathbf{g} by \mathbf{T} , and $m_{1,7,8}^{(0)}$ and $q_{3,5}^{(0)}$ are the equilibrium moments of $m_{1,7,8}$ and $q_{3,5}$ (refer to Appendix B for the expressions). As compared with Eq. (15), the above calculations for \mathbf{S} and $\nabla\phi$ are also local but easier since the second-order moments of distribution functions are avoid.

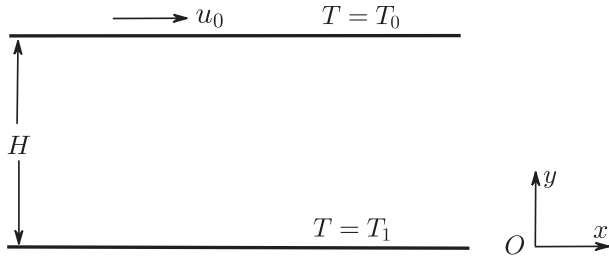


FIG. 1. Schematic of the two-dimensional thermal Couette flow.

Remark 3. As the parameters A and B equal to zero, one can find that the shear rate S will disappear from the present LKS model, while the scalar gradient $\nabla\phi$ still exists in the term of G_i [see Eq. (12)]. This intrinsic difference between Eqs. (4) and (10) brings us a notable result from Eqs. (30) and (31), that is, the present model for the NS equations reduces to the standard BGK model with a single relaxation rate $\frac{1}{\tau_f}$, however, the model for CDE still retains two relaxation rates of $\{\frac{1}{\tau_\phi}, \frac{2}{\tau_\phi + \frac{1}{2}}\}$.

Note that the shear rate S computed by Eq. (15) is dependent on the nonequilibrium part of momentum flux tensor defined by $\Pi_f^{(neq)} = \sum_j c_j c_j (f_j - f_j^{(eq)})$. As a LB model developed for the NS equations, the RLB model [42,43] has some similarities with the present LKS model. That is, the evolution equation is written as the BGK form, and the

nonequilibrium part of momentum flux tensor is included in the evolution equation. Same as the LKS model, it has been demonstrated that the RLB model can improve the accuracy and numerical stability of the BGK model [42,43]. To ascertain and compare the similarity between the present LKS model and the RLB model, we next aim to diagonalize the collision matrix in the generalized evolution equation of RLB model. The RLB model has the following evolution equation [42,43]

$$f_i(\mathbf{x} + \mathbf{c}_i \delta_t, t + \delta_t) = f_i^{(eq)}(\mathbf{x}, t) + \frac{(1 - \frac{1}{\tau_f})\omega_i}{2c_s^4} (\mathbf{c}_i \mathbf{c}_i - c_s^2 \mathbf{I}) : \Pi_f^{(neq)}. \quad (34)$$

Correspondingly, the post-collision distribution functions can be derived

$$f^{post} = f - [f - f^{(eq)}] + \left(1 - \frac{1}{\tau_f}\right) D[f - f^{(eq)}]. \quad (35)$$

Recurring to the invertible matrix T presented in Eq. (25), the above vector equation can be further expressed with diagonalized collision matrix as follows:

$$f^{post} = f - T^{-1} S_{rf} T [f - f^{(eq)}], \quad (36)$$

where $S_{rf} = I - (1 - \frac{1}{\tau_f}) S_D = \text{diag}(1, \frac{1}{\tau_f}, 1, 1, 1, 1, 1, \frac{1}{\tau_f}, \frac{1}{\tau_f})$. Referring to the Chapman-Enskog analysis shown in Appendix B, it can be naturally deduced that the shear and bulk viscosity are computed by $\nu = c_s^2 (\tau_f - \frac{1}{2}) \delta_t$,

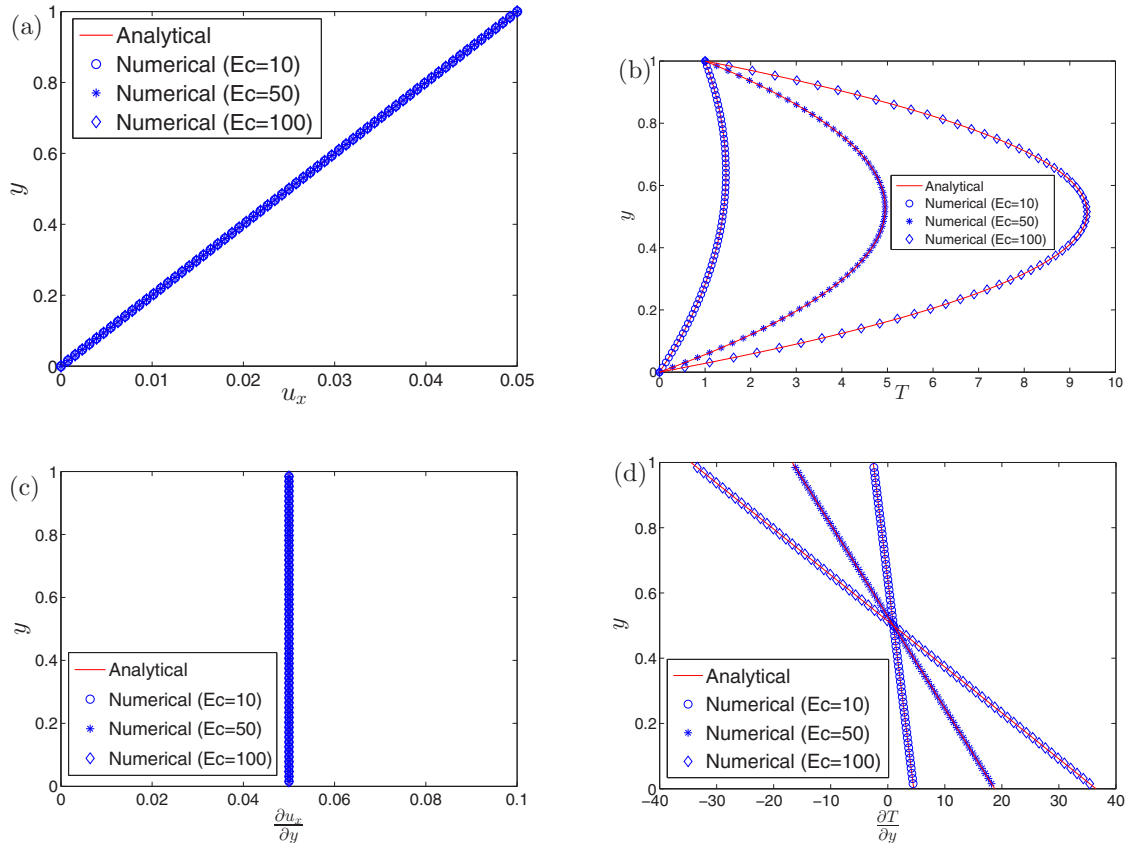


FIG. 2. Comparisons of numerical results [(a) velocity; (b) temperature; (c) velocity gradient; and (d) temperature gradient] and analytical solutions of the thermal Couette flow for different Ec at $Pr = 0.71$. Solid lines: analytical solutions; symbols: numerical results.

TABLE I. Relative errors of velocity \mathbf{u} , temperature T and their gradients under different Eckert numbers at $\text{Pr} = 0.71$.

Ec	$E(u)$	$E(T)$	$E(\partial_y u_x)$	$E(\partial_y T)$
10	1.183×10^{-8}	3.221×10^{-4}	2.188×10^{-8}	8.427×10^{-3}
100	1.183×10^{-8}	5.393×10^{-4}	2.188×10^{-8}	9.339×10^{-3}

$\xi = c_s^2(\tau_f - \frac{1}{2})\delta_t$ in the RLB model. To here, the conclusions can be drawn about the similarity and difference between the RLB model and the present LKS model. Same as the LKS model in this work, the RLB model does not belong to the BGK model since it has two relaxation rates of $\{1, \frac{1}{\tau_f}\}$. This is the essence responsible for its improvement over the BGK model in terms of accuracy and stability. Additionally, it can be found that the relaxation rates of the LKS model and the REG model have the same configuration in the diagonalized collision matrix. However, the shear and bulk viscosities in the RLB model are related with the relaxation time τ_f , while the two viscosities in the present LKS model are determined by an additional parameter A as well as τ_f [see Eq. (9)]. This indicates that the present LKS model could possess more degree of freedom to optimize the numerical stability. In addition, one can find that the relaxation rates for other nonconserved mode in the REG model are all taken to unity, while the corresponding relaxation rates are $\frac{1}{\tau_f}$ in the present LKS model.

Finally, we would like to note that although the proposed LKS model is written as the BGK form in Sec. II B, it can be also performed in the framework of MRT model. Correspondingly, the evolution equations for the NS equations coupled with CDEs are decomposed into two substeps, i.e., collision in moment space and propagation in velocity space,

$$\begin{aligned} \text{Collision: } \quad m_f^{\text{post}} &= m_f - S_f[m_f - m_f^{(\text{eq})}] + \delta_t \tilde{F}, \\ m_g^{\text{post}} &= m_g - S_g[m_g - m_g^{(\text{eq})}] + \delta_t \tilde{G}, \end{aligned} \quad (37)$$

$$\begin{aligned} \text{Propagation: } \quad f_i(\mathbf{x} + \mathbf{c}_i \delta_t, t + \delta_t) &= f_i^{\text{post}}(\mathbf{x}, t), \\ g_i(\mathbf{x} + \mathbf{c}_i \delta_t, t + \delta_t) &= g_i^{\text{post}}(\mathbf{x}, t), \end{aligned} \quad (38)$$

where $m_f = T\mathbf{f}$, $m_g = T\mathbf{g}$ are the moment vectors, $m_f^{(\text{eq})} = T\mathbf{f}^{(\text{eq})}$, $m_g^{(\text{eq})} = T\mathbf{g}^{(\text{eq})}$ are the equilibria in moment space, $m_f^{\text{post}} = T\mathbf{f}^{\text{post}}$, $m_g^{\text{post}} = T\mathbf{g}^{\text{post}}$ are the post-collision moment vectors, and $\tilde{F} = T\hat{F}$, $\tilde{G} = T\hat{G}$. The expressions of $m_f^{(\text{eq})}$, $m_g^{(\text{eq})}$, \tilde{F} and \tilde{G} are definitely given by

TABLE II. Relative errors of velocity \mathbf{u} , temperature T and their gradients with different values of A and Eckert numbers at $\text{Pr} = 0.71$.

A	$10^8 \times E(u)$		$10^4 \times E(T)$		$10^8 \times E(\partial_y u_x)$		$10^3 \times E(\partial_y T)$	
	Ec = 10	Ec = 100	Ec = 10	Ec = 100	Ec = 10	Ec = 100	Ec = 10	Ec = 100
0.01	1.058	1.058	2.281	3.818	1.956	1.956	8.427	9.338
0.1	1.183	1.183	3.221	5.393	2.188	2.188	8.427	9.339
0.2	1.767	1.767	4.266	7.141	3.267	3.267	8.427	9.338
0.3	3.097	3.097	5.309	8.888	5.726	5.726	8.427	9.339
0.4	6.906	6.906	6.351	10.63	12.77	12.77	8.427	9.339

Eqs. (B8)–(B11). Once the two processes are fulfilled at each time step, the macroscopic variables can be computed as Eqs. (7) and (13).

IV. NUMERICAL RESULTS AND DISCUSSIONS

In this section, the present LKS model with the computing schemes for S and $\nabla\phi$ will be validated for the NS equations coupled with CDEs, which contains both the forcing term and the source term. The comparisons between the analytical solutions and present numerical results are made in terms of three well-studied problems with driven external force and heat dissipation, including the planar thermal Posieuille flow, thermal Couette flow with thermal dissipation, and natural convection in a square cavity. In addition, the numerical stability of the present LKS model is investigated and compared with the BGK model.

Unless otherwise stated, the proposed model is implemented in the MRT framework as described above in the simulations. The wall boundary conditions of the NS equations and CDEs is realized by the nonequilibrium extrapolation scheme (NEES) [34,48]. According to the stability conditions of LKS-based models for the NS equations [40], the relaxation times τ_f , also τ_ϕ , should be constrained as $\tau_f \geq \frac{1}{2}$, $\tau_\phi \geq \frac{1}{2}$, and also for the positivity of viscosity and diffusivity, $A \leq \tau_f - \frac{1}{2}$, $B \leq \tau_\phi - \frac{1}{2}$. As the relaxation times are fixed, the parameters A and B are then determined from Eqs. (9) and (14),

$$A = \tau_f - \frac{1}{2} - \frac{\nu}{c_s^2 \delta_t}, \quad B = \tau_\phi - \frac{1}{2} - \frac{D}{c_s^2 \delta_t}. \quad (39)$$

Unless otherwise stated, the relaxation time τ_f and τ_ϕ are both set to be unity.

A. Thermal Couette flow with viscous heat dissipation

Thermal Couette flow with heat dissipation is extensively used as a good test to validate thermal lattice Boltzmann models and thermal boundary conditions. The problem is sketched in Fig. 1 where the top and bottom walls move with different velocities u_0 and 0 in the horizontal direction, and keep at different temperatures T_0 and T_1 , respectively. The velocity and temperature fields of this problem are governed by Eqs. (1) and (2), where the acceleration $\mathbf{a} = \mathbf{0}$ and the source term Q includes the effect of viscous heat dissipation,

$$Q = \frac{\nu}{2C_v} (\mathbf{S} : \mathbf{S}), \quad (40)$$

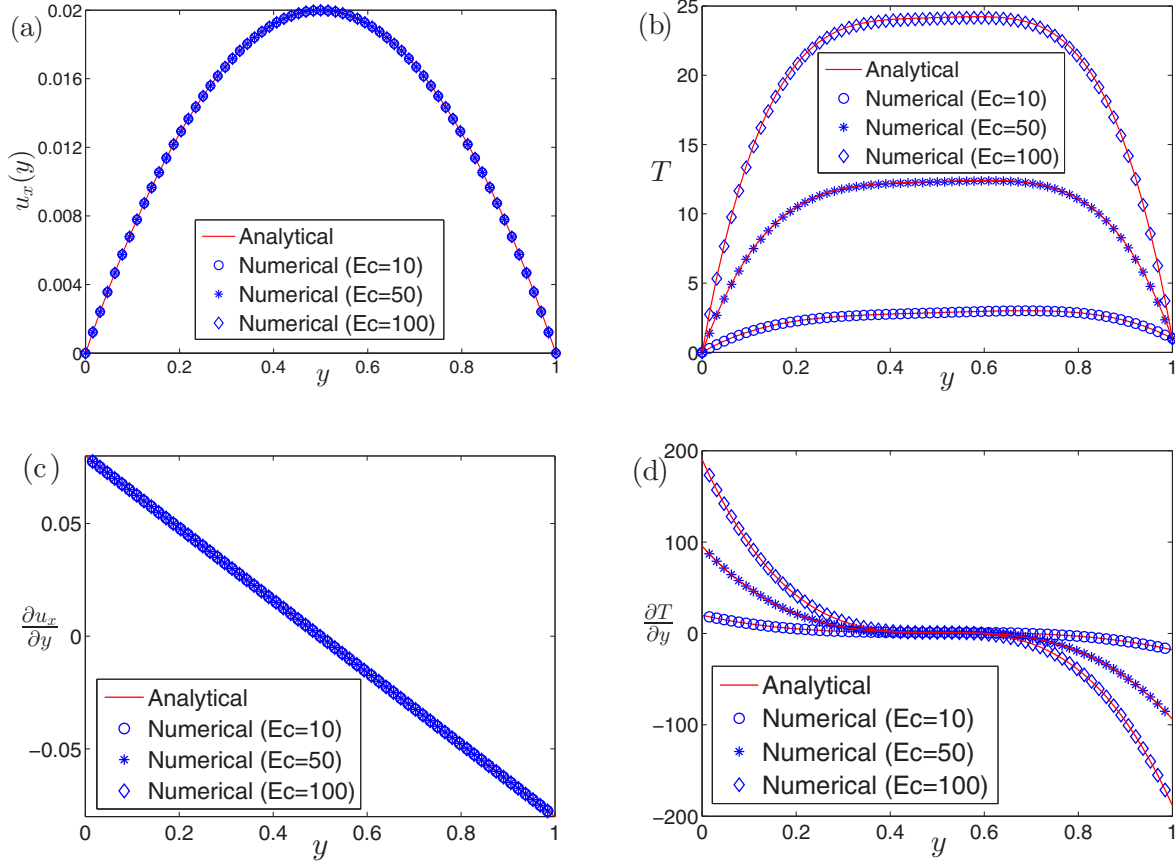


FIG. 3. Comparisons of numerical results [(a) velocity; (b) temperature; (c) velocity gradient and (d) temperature gradient] and analytical solutions of the thermal Poiseuille flow for different Ec at Pr = 0.71 and Re = 20. Solid lines: analytical solutions; symbols: numerical results.

where C_v is the specific heat at constant volume. For better consistent description on this thermal problem, hereafter, the variable ϕ in Eq. (2) is renewed as temperature T .

The problem has the following analytical solutions of velocity $\mathbf{u} = (u_x, u_y)$ and temperature T :

$$u_x(y) = u_0 \frac{y}{H}, \quad u_y = 0, \quad (41)$$

$$\frac{T - T_1}{T_0 - T_1} = \frac{y}{H} + \frac{\text{PrEc}}{2} \frac{y}{H} \left(1 - \frac{y}{H}\right), \quad (42)$$

where Pr and Ec represent the Prandtl number and Eckert number and are defined by

$$\text{Pr} = \frac{\nu}{D}, \quad \text{Ec} = \frac{u_0^2}{C_v(T_0 - T_1)}. \quad (43)$$

From Eqs. (41) and (42), we can also obtain the following gradients of velocity and temperature:

$$\frac{\partial u_x}{\partial y} = \frac{u_0}{H}, \quad \frac{\partial T}{\partial y} = \frac{T_0 - T_1}{H} \left[1 + \frac{\text{PrEc}}{2} \left(1 - \frac{2y}{H}\right)\right]. \quad (44)$$

In the simulations, the physical parameters are set as $H = 1, u_0 = 0.05, T_0 = 1,$ and $T_1 = 0$. The periodic boundary conditions are applied at the inlet and outlet, and the lattice numbers in the vertical direction is first assigned as $N_y = 64$, which is fine enough to obtain accurate results. For this steady problem, the convergence criterion for numerical results to reach the steady state is adopted,

$$\frac{\sum_x |T(\mathbf{x}, t) - T(\mathbf{x}, t - 100\delta_t)|}{\sum_x |T(\mathbf{x}, t)|} < 1.0 \times 10^{-8}. \quad (45)$$

TABLE III. Relative errors of velocity \mathbf{u} , temperature T and their gradients with different Reynolds numbers and Eckert numbers at Pr = 0.71.

Error	Re = 20, Ec = 10	Re = 20, Ec = 100	Re = 100, Ec = 10	Re = 100, Ec = 100
$E(u)$	8.173×10^{-4}	8.173×10^{-4}	8.173×10^{-4}	8.173×10^{-4}
$E(T)$	2.920×10^{-3}	3.563×10^{-3}	2.919×10^{-3}	3.561×10^{-3}
$E(\partial_y u_x)$	9.349×10^{-3}	9.349×10^{-3}	9.349×10^{-3}	9.349×10^{-3}
$E(\partial_y T)$	3.972×10^{-2}	4.007×10^{-2}	3.972×10^{-2}	4.007×10^{-2}

TABLE IV. Relative errors of velocity \mathbf{u} , temperature T , and their gradients with different A and Eckert numbers at $\text{Pr} = 0.71$.

Re	A	$10^4 \times E(u)$		$10^3 \times E(T)$		$10^3 \times E(\partial_y u_x)$		$10^2 \times E(\partial_y T)$	
		Ec = 10	Ec = 100	Ec = 10	Ec = 100	Ec = 10	Ec = 100	Ec = 10	Ec = 100
20	0.01	0.2654	0.2654	1.622	1.931	9.349	9.349	3.972	4.005
	0.1	2.653	2.653	2.035	2.483	9.349	9.349	3.972	4.007
	0.2	5.307	5.307	2.523	3.078	9.349	9.349	3.972	4.007
	0.3	7.960	7.960	3.036	3.704	9.349	9.349	3.972	4.007
	0.4	10.61	10.61	3.575	4.361	9.349	9.349	3.972	4.007

The numerical results against the analytical solutions with different Eckert numbers at $\text{Pr} = 0.71$ are presented in Fig. 2. As shown in the figure, the numerical results associated with velocity, temperature, and their gradients agree well with the corresponding analytical solutions.

Furthermore, a quantitative comparison between numerical results and analytical solutions is performed. To this end, the global relative error (GRE) is used, which is defined as

$$E(\Phi) = \sqrt{\frac{\sum_x |\Phi_a(\mathbf{x}) - \Phi_n(\mathbf{x})|^2}{\sum_x |\Phi_a(\mathbf{x})|^2}}, \quad (46)$$

where Φ_a and Φ_n denote the analytical and numerical results, and the summations cover the entire grid points. The viscosity is kept at the same value in the computations on a grid resolution of $N_y = 64$. Table I lists the GREs at different Eckert numbers. As shown, one can find that the Eckert number has little effect on the GREs of velocity and its gradient, while the GREs associated with temperature and its gradient increase with an increase in Eckert number. This difference can be explained by the following reasons: First, the Eckert number is related with the source term Q [Eq. (40)] through C_v [Eq. (43)], and as a consequence it affects the solutions of temperature fields rather than velocity fields. Second, the effect of viscous heat dissipation is more significant at a larger Ec, which brings a stronger nonlinear distribution of temperature. Another observation in the table is that the GREs of velocity fields are smaller than those of temperature fields. It would be noted that the temperature, based on Eq. (2) and the above discussions, is recognized as a passive scalar influenced by the

velocity. The effects of A and B on the GREs of velocity and temperature are also investigated. For simplicity but without loss of generality, the relaxation time τ_f is fixed at 1.0, A and B are set to be identical ($A \leq \tau_f - 0.5$ as noted before) in the simulations. The computed GREs with different values of A and Eckert numbers are presented in Table II. As expected again, the GREs related with velocity are not influenced by the increase of Eckert number at each A , while the GREs related with temperature become larger. More importantly, it is found that the GREs except for the unchanged $E(\partial_y T)$ increases with the increase of A , which indicates that to derive more accurate results, A (and B) cannot be far larger than zero.

B. Planar thermal Poiseuille flow

The planar thermal Poiseuille flow with heat dissipation is next simulated by the present model. The temperatures on the top and bottom walls are kept at T_0 and T_1 , respectively. The viscous heat dissipation expressed by Eq. (40) is also considered here as the source term Q , while the fluid of this problem in a planar channel is driven by a constant force $\mathbf{F} = \rho(a_x, 0)$.

For the considered problem, the exact solutions of velocity and temperature, and thus their gradients are, respectively, described as

$$u_x(y) = 4U_{\max} \frac{y}{H} \left(1 - \frac{y}{H}\right), \quad u_y = 0, \quad (47)$$

$$\frac{T - T_1}{T_0 - T_1} = \frac{y}{H} + \frac{\text{PrEc}}{3} \left[1 - \left(1 - \frac{2y}{H}\right)^4\right], \quad (48)$$

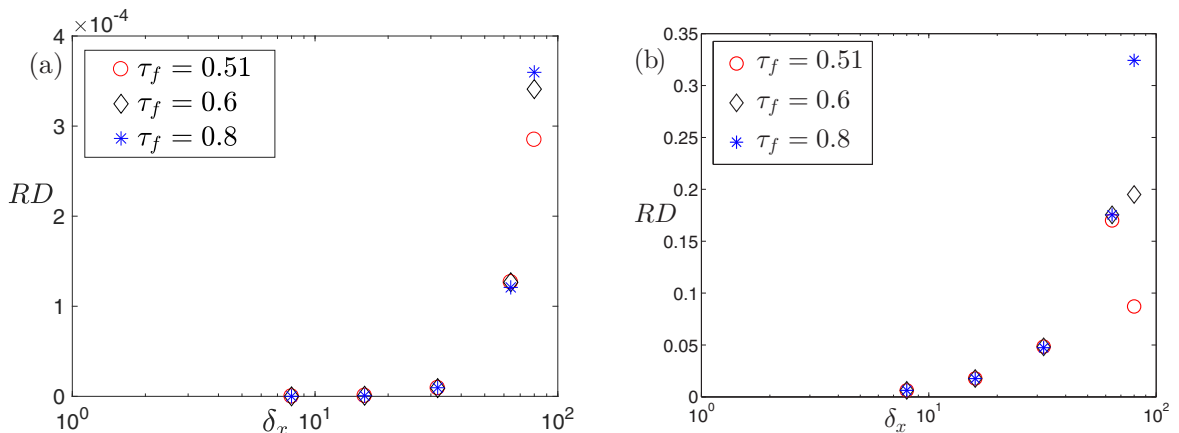


FIG. 4. The relative differences between errors of present model and (a) the previous model [32]; (b) the previous model [33].

TABLE V. The relative differences between errors of the present LKS model and the TRT model.

τ_f	$\delta_x = 1/16$	$\delta_x = 1/32$	$\delta_x = 1/64$	$\delta_x = 1/80$	$\delta_x = 1/100$
0.51	0.0001	0.0005	0.0020	-0.0575	0.0048
0.6	-0.0168	-0.0118	0.0037	0.0149	0.0323
0.8	-0.4921	-0.4411	-0.3838	-0.3511	-0.3008

$$\frac{\partial u_x}{\partial y} = 4 \frac{U_{\max}}{H} \left(1 - 2 \frac{y}{H}\right), \quad (49)$$

$$\frac{\partial T}{\partial y} = \frac{T_0 - T_1}{H} \left[1 + \frac{8\text{PrEc}}{3} \left(1 - \frac{2y}{H}\right)^3\right], \quad (50)$$

where $U_{\max} = a_x H^2 / (8\nu)$ is the maximum velocity, and $\text{Pr} = \nu/D$ is the Prandtl number, and $\text{Ec} = U_{\max}^2 / [C_v(T_0 - T_1)]$ is the Eckert number. It is noted that besides Ec and Pr , the Reynolds number, which is defined by $\text{Re} = U_{\max} H / \nu$, is usually another characterized parameter for the thermal Poiseuille flow. We conducted a set of simulations with different values of Ec at $\text{Pr} = 0, 71$, $\text{Re} = 20$, $T_0 = 1$ and $T_1 = 0$. In the computations, an 8×64 lattice is used, and the boundary treatment is identical to that employed in the Couette flow. In Fig. 3, the profiles of velocity, temperature and their gradients are presented together with the analytical solutions. From this figure, one can observe an excellent agreement between the numerical results and the analytical solutions. Furthermore, a quantitative evaluation on the difference between the numerical results and the analytical solutions is performed, and the GREs at different Reynolds numbers and Eckert numbers are calculated. Here, the Reynolds numbers are obtained by fixing the viscosity while changing the acceleration a_x , and the Eckert numbers are obtained by changing the corresponding C_v . As seen in Table III, increasing the Eckert number does not alter the GREs of velocity while increases the GREs of temperature, which is consistent with the thermal Couette flow. In addition, the GREs of velocity and temperature both keep unchanged as the Reynolds number increases. The influence of A and B on the deviation of numerical results from analytical solutions is also investigated. Note that the relative errors are not affected by the Reynolds number. The case as $\text{Re} = 20$ is only considered in the simulations. The four GREs of velocity and temperature are shown in Table IV. The relaxation time τ_f is set as $\tau_f = 1.0$, and the parameters of A and B take the same value as adopted previously. The numerical outcome in the Table indicates that as the value of A increases, the GREs of velocity and temperature increase, while the GREs of their gradients are kept unchanged.

In addition to the locality of numerical implementation in time and space, the present LKS model satisfies the consistency accurately with the NS equations coupled with CDEs via the Chapman-Enskog analysis presented in Appendix B. From this point of view, the present LKS model could be considered as a modified version of existing LKS models. In the following, we will compare the present LKS model and previous ones [32,33] in terms of relative difference. For a quantitative comparison, the relative difference (RD) between errors of the present model and the existing models

is employed, which is defined as follows

$$\text{RD} = \frac{E(\tilde{\Phi}) - E(\Phi)}{E(\Phi)}, \quad (51)$$

where $E(\Phi)$ and $E(\tilde{\Phi})$ denote the GREs of the present model and the existing model. In the simulations here, the compared models are implemented in the BGK framework, and the dimensionless parameters are used as $\text{Pr} = 0.71$, $\text{Re} = 20$, $\text{Ec} = 100$. Note that the evolution equation for flow fields are identical in the three models. Figure 4 only presents the relative differences from temperature at different relaxation times and grid sizes. As seen from the figure, the relative differences are both larger than zero, as expected, since the present model is theoretically not less accurate than previous LKS models. And additionally, it is also found that there is no much difference between the results obtained from the present model and the previous models in Refs. [32,33]. This conforms the fact that the present local model can ensure deriving the macroscopic equations correctly. Furthermore, we computed the RDs shown in Table V to compare the present LKS model with the TRT model which was verified against the analytical solutions. From this Table, one can find that the relative differences between the present model and the TRT model are relatively small, which indicates the overall consistency between these two models.

C. Natural convection in a square cavity

Natural convection flow in a square cavity is further considered to investigate the numerical stability of present model for the NS equations coupled with CDEs. The schematic of the problem is shown in Fig. 5, where the upper and lower walls of the cavity are insulated, while the left and

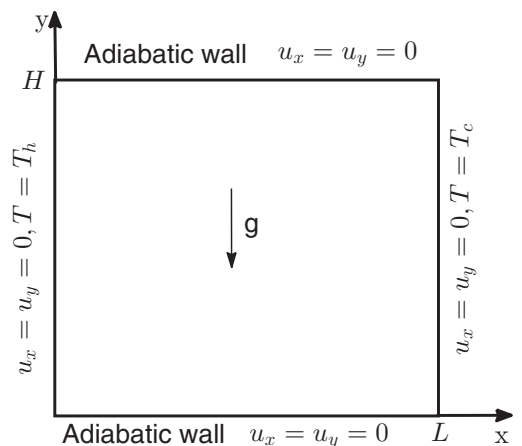


FIG. 5. Schematic of natural convection in a fluid-saturated porous cavity.

TABLE VI. Comparisons of the numerical results by the present LKS model with the benchmark solutions [49,50] and the reported LB data [32,51] ($Pr = 0.71$, and grid sizes: 100×100 for $Ra = 10^3$, 150×150 for $Ra = 10^4$, and 200×200 for $Ra = 10^5$, $Ra = 10^6$).

$Ra(N_x \times N_y)$		u_{\max}	y_{\max}	v_{\max}	x_{\max}	Nu_{\max}	y_{Nu}	\bar{Nu}
10^3 (100×100)	Ref. [49]	3.649	0.813	3.697	0.178	–	–	–
	Ref. [51]	3.6554	0.8125	3.6985	0.1797	1.5004	0.90625	1.1168
	Ref. [32]	3.652	–	3.703	–	1.508	–	1.115
	Present	3.6353	0.8100	3.7019	0.1800	1.5089	0.9100	1.1182
10^4 (150×150)	Ref. [50]	16.1802	0.8265	19.6295	0.1193	3.5309	0.8531	2.2448
	Ref. [51]	16.0761	0.8203	19.6368	0.1172	3.5715	0.8594	2.2477
	Ref. [32]	16.171	–	19.622	–	3.543	–	2.247
	Present	16.1672	0.8267	19.6251	0.1200	3.5410	0.8600	2.2469
10^5 (200×200)	Ref. [50]	34.7399	0.8558	68.6396	0.0657	7.7201	0.9180	4.5216
	Ref. [51]	34.8343	0.8594	68.2671	0.0625	7.7951	0.9219	4.5345
	Ref. [32]	34.813	–	68.550	–	7.762	–	4.544
	Present	34.9921	0.8550	68.4594	0.0650	7.7561	0.9250	4.5197
10^6 (200×200)	Ref. [50]	64.8367	0.8505	220.461	0.0390	17.5360	0.9608	8.8251
	Ref. [51]	65.3606	0.8516	216.415	0.0391	17.4836	0.9688	8.7775
	Ref. [32]	64.675	–	220.135	–	17.640	–	8.813
	Present	65.1668	0.8500	218.6811	0.0400	17.5728	0.9650	8.770

right walls are maintained at different temperatures T_h and T_c ($T_h > T_c$), respectively. The zero velocity boundary condition is satisfied at the walls of the cavity. The height and width of the cavity are H and L , and the temperature difference and the reference temperature are $\Delta T = T_h - T_c$ and $T_0 = (T_h + T_c)/2$ respectively. With the Boussinesq approximation, the fluid properties are considered as constant except that the fluid density is linearly dependent with temperature in the buoyancy force. Thus, the acceleration vector \mathbf{a} in Eq. (1b) may be rewritten as $\mathbf{a} = g\beta(T - T_0)\mathbf{j}$, where g is the gravity acceleration, β is the coefficient of thermal expansion, and \mathbf{j} is the unit vector in the opposite direction of gravity. Besides the Prandtl number, another main dimensionless parameter to character this problem is the Rayleigh number Ra defined by $Ra = g\beta\Delta TH^3/(\nu D)$. The average Nusselt number \bar{Nu} on

the left (or right) vertical wall is defined as

$$\bar{Nu} = \frac{1}{H} \int_0^H Nu(y) dy, \quad (52)$$

where $Nu(y) = -L(\partial T/\partial x)_{\text{wall}}/\Delta T$ is the local Nusselt number. Some simulations are first carried out to validate the present model. For quantitative comparisons with previous benchmark solutions, the maximum horizontal velocity component u_{\max} at the mid-width ($x = L/2$) and its location y_{\max} , the maximum vertical velocity component v_{\max} at the mid-height ($y = H/2$) and its location x_{\max} , the maximum Nusselt number Nu_{\max} and the corresponding location y_{Nu} , and the average Nusselt number \bar{Nu} along the cold wall are computed and listed in Table VI. In the simulations, Pr is set to be 0.71, and the lattice sizes are chosen differently with Ra :

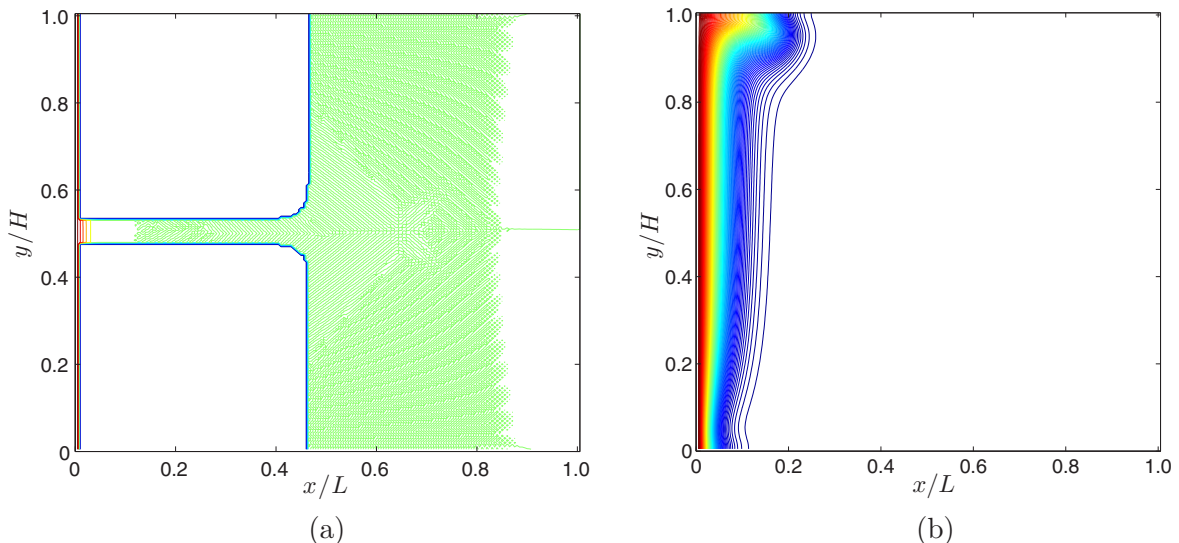


FIG. 6. Isotherms of the natural convection in a cavity. The results are obtained by (a) the standard BGK model at $t = 2000\delta_t$, and (b) the present model at $t = 2000\delta_t$.

100×100 for $Ra = 10^3$, 150×150 for $Ra = 10^4$, 10^5 , and 200×200 for 10^6 . As shown in the table, the present computed results are in good agreement with the benchmark data for all the considered values of Ra .

The numerical stability of the present modified LKS model is next examined and compared with the BGK model. Considering that the present model can correctly recover the macroscopic equations, the BGK model which is reduced from our model by taking $A = 0$ and $B = 0$ is adopted for comparison. It is well known that the numerical instability will occur for the BGK model when the relaxation times are close to 0.5. By contrast, the present model, as noted in previous section, can possess superior stability due to the essence that it has two relaxation times. To see this more clearly, a set of simulations as τ_f approaches to 0.5 are then performed on a 200×200 lattice at $Ra = 10^6$, and the other computational conditions are the same as above. It is found that for the standard BGK model at $\nu = 1.3333 \times 10^{-4}$ ($\tau_f = 0.58$), the numerical oscillation occurs when $t = 200\delta_t$ [see Fig. 6(a)], and eventually the computation blows up as $t = 300\delta_t$. While the isotherm of the present LKS model at the same viscosity ($\tau_f = 0.75$) is stable and smooth even at $t = 2000\delta_t$ [see Fig. 6(b)], and finally evolves to the steady state. Moreover, the computed values of u_{\max} , y_{\max} , v_{\max} , x_{\max} , Nu_{\max} , y_{Nu} , \bar{Nu} are 66.2989, 0.8550, 219.9009, 0.0400, 17.4653, 0.9650, 8.6928, respectively, which departure less than 2.25% from the benchmark data. This indicates that the present model is more stable than the standard BGK model. To reinforce this point, the capacity of the present model are further tested at smaller fluid viscosities. We found that the present model is still accurate and stable even as $\nu = 8.3333 \times 10^{-6}$ (corresponds to $\tau_f = 0.505$ in the BGK model). The respective values of u_{\max} , y_{\max} , v_{\max} , x_{\max} , Nu_{\max} , y_{Nu} , \bar{Nu} are 67.4338, 0.8550, 222.4333, 0.0400, 16.9509, 0.9650, 8.4646, which deviate within 5% from the benchmark results. Additionally, in view of the fixed Prandtl number in the simulations, we would like to point out that better numerical stability of the present model for CDE is actually verified as τ_ϕ approaches to 0.5. The above results clearly demonstrate the superior stability of the present model over the BGK model, which is attributed to the larger degree of freedom from two relaxation times.

V. CONCLUSIONS

The LKS has been incorporated in the LB models to improve the numerical stability in simulations of the NS equations coupled with CDEs. However, there are two basic issues within the modified LKS models in the literature. One is that the NS equations coupled with CDEs with the source term in Cartesian coordinate are not accurately derived from the models which can be implemented locally in time and space. The other is that whether the modified LKS models should be grouped to the BGK model is still unresolved. Targeting these two issues, a LB model based on the LKS is presented for the NS equations coupled with CDEs. The shear rate and scalar gradient contained in the model are computed by the local nonequilibrium scheme, which ensures the locality of collision process of the present model. The Chapman-Enskog

analysis demonstrates that the NS equations coupled with CDEs can be correctly recovered from the present model without any additional assumptions. Subsequently, a transformation matrix is carefully designed to diagonalize the two collision matrices extracted in the generalized LBE. It is hence found that the diagonal matrices have only two groups of eigenvalues. This definitely proves that the present modified LKS model for the NS equations coupled with CDEs is actually not a BGK model but has two relaxation rates, which clarifies the essence of better numerical stability from modified LKS models.

Several benchmark tests are simulated to validate the present model and the local scheme for the gradient terms. For the planar thermal Poiseuille flow, the present LKS model is compared with previous LKS models, and we found that the present model is not less accurate than previous ones. For the natural convection in a cavity, the present LKS model is found to be much more stable than the BGK model. These results are consistent with and confirm our theoretical results. Additionally, following the theoretical proof shown in this work, it was definitely proved that the RLB model [42,43] is not a BGK model but has two relaxation times as the present LKS model. Based on this, we would like to note that the regularized LB model and its variants should be of the same kind with the modified local LKS model. In addition, according to the diagonalized collision matrix of the RLB model, we would like to note that the present LKS model could possess more degree of freedom to optimize the numerical stability.

ACKNOWLEDGMENTS

This work is financially supported by the National Natural Science Foundation of China under Grant No. 51776068, the National Science Fund for Distinguished Young Scholars of China under Grant No. 51525602, the National Natural Science Foundation of China under Grant No. 11602075, and the Fundamental Research Funds for the Central Universities under Grant No. 2018MS060. The second author (W.-F. Zhao) was supported by the China Postdoctoral Science Foundation (Grant No. 2017M620603) and Fundamental Research Funds for the Central Universities (Grant No. FRF-TP-17-068A1). L. Wang is indebted to Profs. Wen-an Yong and Zhaoli Guo for insightful discussions.

APPENDIX A: BASIC RESULTS ON THE MATRICES D AND R

In this Appendix, we will prove the matrices D and R satisfy $D^2 = D$ and $R^2 = R$. Mathematically, it can be turned to prove $\sum_k D_{i,k} D_{k,j} = D_{ij}$ and $\sum_k R_{i,k} R_{k,j} = R_{ij}$. Before proceeding further, the following facts accompanied with the D2Q9 lattice model should be cleared:

$$\sum_i \omega_i c_{i,\alpha} c_{i,\beta} = c_s^2 \delta_{\alpha\beta}, \quad \sum_i \omega_i c_{i,\alpha} c_{i,\beta} c_{i,\gamma} c_{i,\theta} = c_s^4 \Delta_{\alpha\beta\gamma\theta}, \quad (\text{A1})$$

where $\Delta_{\alpha\beta\gamma\theta} = \delta_{\alpha\beta} \delta_{\gamma\theta} + \delta_{\alpha\gamma} \delta_{\beta\theta} + \delta_{\alpha\theta} \delta_{\beta\gamma}$, where $c_{k,s}$ ($s = \alpha, \beta, \gamma$, or θ) is the component of c_k along the s direction, and $\delta_{\alpha\beta}$ is the Kronecker δ with two indices of α and β .

We then base the above results with Eq. (21) to deduce

$$\begin{aligned}
\sum_k D_{i,k} D_{k,j} &= \sum_k \omega_i \frac{1}{2c_s^4} [\mathbf{c}_k \mathbf{c}_k : (\mathbf{c}_i \mathbf{c}_i - c_s^2 \mathbf{I})] \times \omega_k \frac{1}{2c_s^4} [\mathbf{c}_j \mathbf{c}_j : (\mathbf{c}_k \mathbf{c}_k - c_s^2 \mathbf{I})] \\
&= \omega_i \frac{1}{4c_s^8} \sum_k \omega_k c_{k,\alpha} c_{k,\beta} (c_{i,\beta} c_{i,\alpha} - c_s^2 \delta_{\beta\alpha}) c_{j,\gamma} c_{j,\theta} (c_{k,\theta} c_{k,\gamma} - c_s^2 \delta_{\theta\gamma}) \\
&= \omega_i \frac{1}{4c_s^4} [c_{j,\gamma} c_{j,\theta} (c_{i,\beta} c_{i,\alpha} - c_s^2 \delta_{\beta\alpha}) \delta_{\alpha\gamma} \delta_{\beta\theta} + c_{j,\gamma} c_{j,\theta} (c_{i,\beta} c_{i,\alpha} - c_s^2 \delta_{\beta\alpha}) \delta_{\alpha\theta} \delta_{\beta\gamma}] \\
&= \omega_i \frac{1}{2c_s^4} c_{j,\alpha} c_{j,\beta} (c_{i,\beta} c_{i,\alpha} - c_s^2 \delta_{\beta\alpha}) = \omega_i \frac{1}{2c_s^4} [\mathbf{c}_j \mathbf{c}_j : (\mathbf{c}_i \mathbf{c}_i - c_s^2 \mathbf{I})] = D_{i,j}.
\end{aligned} \tag{A2}$$

This clearly indicates to us that $\mathbf{D}^2 = \mathbf{D}$.

Similarly, for the matrix \mathbf{R} with Eq. (21), one can obtain that

$$\sum_k R_{i,k} R_{k,j} = \sum_k \omega_i \frac{1}{c_s^2} \mathbf{c}_i \cdot \mathbf{c}_k \times \omega_k \frac{1}{c_s^2} \mathbf{c}_k \cdot \mathbf{c}_j = \omega_i \frac{1}{c_s^4} \sum_k \omega_k c_{i,\alpha} c_{k,\alpha} c_{k,\beta} c_{j,\beta} = \omega_i \frac{1}{c_s^2} c_{i,\alpha} c_{j,\beta} \delta_{\beta\alpha} = \omega_i \frac{1}{c_s^2} \mathbf{c}_i \cdot \mathbf{c}_j = R_{i,j}, \tag{A3}$$

which proves $\mathbf{R}^2 = \mathbf{R}$.

Finally, we come to determine the traces of \mathbf{D} and \mathbf{R} , which equal to the summation of the diagonal entries. Still with Eq. (21), we have

$$\text{tr}(\mathbf{D}) = \sum_i D_{ii} = \sum_i \omega_i \frac{1}{2c_s^4} [\mathbf{c}_i \mathbf{c}_i : (\mathbf{c}_i \mathbf{c}_i - c_s^2 \mathbf{I})] = \sum_i \omega_i \frac{1}{2c_s^4} c_{i,\alpha} c_{i,\beta} (c_{i,\beta} c_{i,\alpha} - c_s^2 \delta_{\beta\alpha}) = \frac{1}{2} (\delta_{\alpha\beta} \delta_{\beta\alpha} + \delta_{\alpha\alpha} \delta_{\beta\beta}) = 3, \tag{A4}$$

and

$$\text{tr}(\mathbf{E}) = \sum_i E_{ii} = \sum_i \omega_i \frac{1}{c_s^2} \mathbf{c}_i \cdot \mathbf{c}_i = \frac{1}{c_s^2} \sum_i \omega_i c_{i,\alpha} c_{i,\alpha} = \delta_{\alpha\alpha} = 2, \tag{A5}$$

where the Einstein summation convention is employed for the subscripts α and β .

APPENDIX B: CHAPMAN-ENSKOG ANALYSIS OF THE PRESENT LKS MODEL

The Chapman-Enskog analysis is now performed on the generalized LBE of the present model to demonstrate its consistency with Eqs. (4) and (10). Referencing to Eqs. (17) and (18), the evolution equations of the present model is written as the following general form

$$\mathbf{f}(\mathbf{x} + \mathbf{c}\delta_t, t + \delta_t) - \mathbf{f}(\mathbf{x}, t) = -\frac{1}{\tau_f} [\mathbf{f} - \mathbf{f}^{(\text{eq})}] + \frac{A}{\tau_f(A - \tau_f)} \mathbf{D}[\mathbf{f} - \mathbf{f}^{(\text{eq})}] + \delta_t \hat{\mathbf{F}}, \tag{B1}$$

$$\mathbf{g}(\mathbf{x} + \mathbf{c}\delta_t, t + \delta_t) - \mathbf{g}(\mathbf{x}, t) = -\frac{1}{\tau_\phi} [\mathbf{g} - \mathbf{g}^{(\text{eq})}] + \frac{B + \tau_\phi - \frac{1}{2}}{\tau_\phi(B - \tau_\phi - \frac{1}{2})} \mathbf{R}[\mathbf{g} - \mathbf{g}^{(\text{eq})}] + \delta_t \hat{\mathbf{G}}, \tag{B2}$$

where two nine-dimensional column vectors are introduced

$$\begin{aligned}
\mathbf{f}(\mathbf{x} + \mathbf{c}\delta_t, t + \delta_t) &:= (f_0(\mathbf{x}, t), f_1(\mathbf{x} + \mathbf{c}_1\delta_t, t), \dots, f_8(\mathbf{x} + \mathbf{c}_8\delta_t, t))^T, \\
\mathbf{g}(\mathbf{x} + \mathbf{c}\delta_t, t + \delta_t) &:= (g_0(\mathbf{x}, t), g_1(\mathbf{x} + \mathbf{c}_1\delta_t, t), \dots, g_8(\mathbf{x} + \mathbf{c}_8\delta_t, t))^T.
\end{aligned}$$

Then, applying the Taylor expansion to the first two terms of each above equations and employing Eqs. (29)–(31), we can obtain

$$\mathbf{D}\mathbf{f} + \frac{\delta_t}{2} \mathbf{D}^2 \mathbf{f} = -\mathbf{T}^{-1} \mathbf{S}'_f \mathbf{T} [\mathbf{f} - \mathbf{f}^{(\text{eq})}] + \hat{\mathbf{F}}, \tag{B3}$$

$$\mathbf{D}\mathbf{g} + \frac{\delta_t}{2} \mathbf{D}^2 \mathbf{g} = -\mathbf{T}^{-1} \mathbf{S}'_g \mathbf{T} [\mathbf{g} - \mathbf{g}^{(\text{eq})}] + \hat{\mathbf{G}}, \tag{B4}$$

where $\mathbf{D} = \partial_t \mathbf{I} + \mathbf{C}_\alpha \partial_\alpha$, $\mathbf{C}_\alpha = \text{diag}(c_{0,\alpha}, c_{1,\alpha}, \dots, c_{8,\alpha})$, $\mathbf{S}'_f = \mathbf{S}_f / \delta_t$ and $\mathbf{S}'_g = \mathbf{S}_g / \delta_t$. As usually done in the MRT model [52], multiplying the transformation matrix \mathbf{T} on both sides of Eqs. (B3) and (B4), one can easily obtain the corresponding equations in moment space,

$$\tilde{\mathbf{D}}\mathbf{m}_f + \frac{\delta_t}{2} \tilde{\mathbf{D}}^2 \mathbf{m}_f = -\mathbf{S}'_f [\mathbf{m}_f - \mathbf{m}_f^{(\text{eq})}] + \tilde{\mathbf{F}}, \tag{B5}$$

$$\tilde{\mathbf{D}}\mathbf{m}_g + \frac{\delta_t}{2} \tilde{\mathbf{D}}^2 \mathbf{m}_g = -\mathbf{S}'_g [\mathbf{m}_g - \mathbf{m}_g^{(\text{eq})}] + \tilde{\mathbf{G}}, \tag{B6}$$

where $\tilde{\mathbf{D}} = \mathbf{T}\mathbf{D}\mathbf{T}^{-1} = \partial_t \mathbf{I} + \tilde{\mathbf{C}}_\alpha \partial_\alpha$ and $\tilde{\mathbf{C}}_\alpha = \mathbf{T}\mathbf{C}_\alpha \mathbf{T}^{-1}$, and \mathbf{m}_f , \mathbf{m}_g , $\mathbf{m}_f^{(\text{eq})}$, $\mathbf{m}_g^{(\text{eq})}$ together with $\tilde{\mathbf{F}}$ and $\tilde{\mathbf{G}}$ are several moment vectors mapped from the corresponding vectors in velocity space by the matrix \mathbf{T} , which are, respectively, given by

$$\mathbf{m}_f = \mathbf{T}\mathbf{f} = (m_{f0}, m_{f1}, \dots, m_{f8})^T, \quad \mathbf{m}_g = \mathbf{T}\mathbf{g} = (m_{g0}, m_{g1}, \dots, m_{g8})^T, \quad (\text{B7})$$

$$\mathbf{m}_f^{(\text{eq})} = \mathbf{T}\mathbf{f}^{(\text{eq})} = (\rho, \rho(2 + 3\mathbf{u}^2), -\rho, \rho u_x, 0, \rho u_y, 0, \rho(u_x^2 - u_y^2), \rho u_x u_y)^T, \quad (\text{B8})$$

$$\mathbf{m}_g^{(\text{eq})} = \mathbf{T}\mathbf{g}^{(\text{eq})} = (\phi, \phi(4 + 3\mathbf{u}^2), -2\phi, \phi u_x, 0, \phi u_y, 0, \phi(u_x^2 - u_y^2), \phi u_x u_y)^T, \quad (\text{B9})$$

$$\tilde{\mathbf{F}} = \mathbf{T}\hat{\mathbf{F}} = \left\{ 0, 6 \left[1 + \frac{1}{2(A - \tau_f)} \right] \rho \mathbf{a} \cdot \mathbf{u}, 0, \left(1 - \frac{1}{2\tau_f} \right) \rho a_x, 0, \left(1 - \frac{1}{2\tau_f} \right) \rho a_y, 0, \right. \\ \left. 2 \left[1 + \frac{1}{2(A - \tau_f)} \right] \rho (a_x u_x - a_y u_y), \left[1 + \frac{1}{2(A - \tau_f)} \right] \rho (a_x u_y + a_y u_x) \right\}^T, \quad (\text{B10})$$

$$\tilde{\mathbf{G}} = \mathbf{T}\hat{\mathbf{G}} = \left\{ \left(1 - \frac{1}{2\tau_g} \right) Q, 2 \left(1 - \frac{1}{2\tau_\phi} \right) Q, - \left(1 - \frac{1}{2\tau_\phi} \right) Q, \left[1 - \frac{1}{\tau_\phi - B + \frac{1}{2}} \right] (\phi a_x + Q u_x), \right. \\ \left. 0, \left[1 - \frac{1}{\tau_\phi - B + \frac{1}{2}} \right] (\phi a_y + Q u_y) \right\}^T. \quad (\text{B11})$$

To here, the involved multiscale expansions are introduced

$$\mathbf{m}_f = \sum_{n=0}^{\infty} \varepsilon^{(n)} \mathbf{m}_f^{(n)}, \quad \mathbf{m}_g = \sum_{n=0}^{\infty} \varepsilon^{(n)} \mathbf{m}_g^{(n)}, \quad (\text{B12a})$$

$$\partial_t = \varepsilon \partial_{t_0} + \varepsilon^2 \partial_{t_1}, \quad \partial_\alpha = \varepsilon \partial_{0\alpha}, \quad (\text{B12b})$$

$$\mathbf{a} = \varepsilon \mathbf{a}_1, \quad Q = \varepsilon Q_1, \quad (\text{B12c})$$

where ε is a small parameter and $\mathbf{a}_1 = (a_{1x}, a_{1y})$. Applying (B12c) to Eqs. (B10) and (B11), it can also assume that $\tilde{\mathbf{F}} = \varepsilon \tilde{\mathbf{F}}_1$ and $\tilde{\mathbf{G}} = \varepsilon \tilde{\mathbf{G}}_1$.

Substituting Eqs. (B12) into Eqs. (B5) and (B6), we can obtain the consecutive orders of Eqs. (B5) and (B6) in terms of ε

$$\varepsilon^0 : \mathbf{m}_f^{(0)} = \mathbf{m}_f^{(\text{eq})}, \quad (\text{B13a})$$

$$\varepsilon^1 : \tilde{\mathbf{D}}_0 \mathbf{m}_f^{(0)} = -\mathbf{S}'_f \mathbf{m}_f^{(1)} + \tilde{\mathbf{F}}_1, \quad (\text{B13b})$$

$$\varepsilon^2 : \partial_{t_1} \mathbf{m}_f^{(0)} + \tilde{\mathbf{D}}_0 \mathbf{m}_f^{(1)} + \frac{\delta_t}{2} \tilde{\mathbf{D}}_0^2 \mathbf{m}_f^{(0)} = -\mathbf{S}'_f \mathbf{m}_f^{(2)}, \quad (\text{B13c})$$

$$\varepsilon^0 : \mathbf{m}_g^{(0)} = \mathbf{m}_g^{(\text{eq})}, \quad (\text{B13d})$$

$$\varepsilon^1 : \tilde{\mathbf{D}}_0 \mathbf{m}_g^{(0)} = -\mathbf{S}'_g \mathbf{m}_g^{(1)} + \tilde{\mathbf{G}}_1, \quad (\text{B13e})$$

$$\varepsilon^2 : \partial_{t_1} \mathbf{m}_g^{(0)} + \tilde{\mathbf{D}}_0 \mathbf{m}_g^{(1)} + \frac{\delta_t}{2} \tilde{\mathbf{D}}_0^2 \mathbf{m}_g^{(0)} = -\mathbf{S}'_g \mathbf{m}_g^{(2)}, \quad (\text{B13f})$$

where $\tilde{\mathbf{D}}_0 = \partial_{t_0} \mathbf{I} + \tilde{\mathbf{C}}_\alpha \partial_{0\alpha}$. Further, rewriting the third terms of Eqs. (B13c) and (B13f), respectively, by Eqs. (B13b) and (B13e) yields

$$\partial_{t_1} \mathbf{m}_f^{(0)} + \tilde{\mathbf{D}}_0 \left(\mathbf{I} - \frac{\mathbf{S}'_f}{2} \right) \mathbf{m}_f^{(1)} + \frac{\delta_t}{2} \tilde{\mathbf{D}}_0 \tilde{\mathbf{F}}_1 = -\mathbf{S}'_f \mathbf{m}_f^{(2)}, \quad (\text{B14a})$$

$$\partial_{t_1} \mathbf{m}_g^{(0)} + \tilde{\mathbf{D}}_0 \left(\mathbf{I} - \frac{\mathbf{S}'_g}{2} \right) \mathbf{m}_g^{(1)} + \frac{\delta_t}{2} \tilde{\mathbf{D}}_0 \tilde{\mathbf{G}}_1 = -\mathbf{S}'_g \mathbf{m}_g^{(2)}. \quad (\text{B14b})$$

Based on Eq. (B12a) and combining Eqs. (7) and (13) with Eqs. (B13a) and (B13d), we can derive

$$m_{f0}^{(k)} = 0 (k > 0), \quad m_{f3}^{(k)} = m_{f5}^{(k)} = 0 (k > 1), \quad (\text{B15a})$$

$$m_{f3}^{(1)} = -\frac{\delta_t}{2} \rho a_{1x}, \quad m_{f5}^{(1)} = -\frac{\delta_t}{2} \rho a_{1y}, \quad (\text{B15b})$$

$$m_{g0}^{(k)} = 0 (k > 1), \quad m_{g0}^{(1)} = -\frac{\delta_t}{2} Q_1. \quad (\text{B15c})$$

1. Derivation of the Navier-Stokes equations

At the t_0 timescale, the moment equation, Eq. (B13b), can be explicitly rewritten as

$$\partial_{t_0} \begin{pmatrix} \rho \\ \rho(2 + 3\mathbf{u}^2) \\ -\rho \\ \rho u_x \\ 0 \\ \rho u_y \\ 0 \\ \rho(u_x^2 - u_y^2) \\ \rho u_x u_y \end{pmatrix} + \partial_{0x} \begin{pmatrix} \rho u_x \\ 4\rho u_x \\ -\rho u_x \\ \frac{1}{3}\rho + \rho u_x^2 \\ \rho u_y^2 \\ \rho u_x u_y \\ 2\rho u_x u_y \\ \frac{2}{3}\rho u_x \\ \frac{1}{3}\rho u_y \end{pmatrix} + \partial_{0y} \begin{pmatrix} \rho u_y \\ 4\rho u_y \\ -\rho u_y \\ \rho u_x u_y \\ 2\rho u_x u_y \\ \frac{1}{3}\rho + \rho u_y^2 \\ \rho u_x^2 \\ -\frac{2}{3}\rho u_y \\ \frac{1}{3}\rho u_x \end{pmatrix} = \begin{pmatrix} 0 \\ -\frac{1}{(\tau_f - A)\delta_t} m_{f1}^{(1)} \\ -\frac{1}{\tau_f \delta_t} m_{f2}^{(1)} \\ \frac{1}{2\tau_f} \rho a_{1x} \\ -\frac{1}{\tau_f \delta_t} m_{f4}^{(1)} \\ \frac{1}{2\tau_f} \rho a_{1y} \\ -\frac{1}{\tau_f \delta_t} m_{f6}^{(1)} \\ -\frac{1}{(\tau_f - A)\delta_t} m_{f7}^{(1)} \\ -\frac{1}{(\tau_f - A)\delta_t} m_{f8}^{(1)} \end{pmatrix} + \begin{pmatrix} 6 \left[1 - \frac{1}{2(\tau_f - A)} \right] \rho \mathbf{a}_1 \cdot \mathbf{u} \\ 0 \\ \left(1 - \frac{1}{2\tau_f} \right) \rho a_{1x} \\ 0 \\ \left(1 - \frac{1}{2\tau_f} \right) \rho a_{1y} \\ 0 \\ \left[1 - \frac{1}{2(\tau_f - A)} \right] \rho (a_{1x} u_x - a_{1y} u_y) \\ \left[1 - \frac{1}{2(\tau_f - A)} \right] \rho (a_{1x} u_y + a_{1y} u_x) \end{pmatrix}. \quad (\text{B16})$$

Similarly, we can rewrite Eq. (B14a) concretely at the t_1 timescale and only present the equations corresponding to the conserved moments ρ and $\rho\mathbf{u}$:

$$\partial_{t_1}\rho = 0, \quad (\text{B17a})$$

$$\begin{aligned} \partial_{t_1}(\rho u_x) + \partial_{0x} \left[\frac{1}{6} \left(1 - \frac{1}{2(\tau_f - A)} \right) m_{f1}^{(1)} + \frac{1}{2} \left(1 - \frac{1}{2(\tau_f - A)} \right) m_{f7}^{(1)} \right] + \partial_{0y} \left[\left(1 - \frac{1}{2(\tau_f - A)} \right) m_{f8}^{(1)} \right] \\ + \delta_t \partial_{0x} \left[1 - \frac{1}{2(\tau_f - A)} \right] \rho u_x a_{1x} + \frac{\delta_t}{2} \partial_{0y} \left[1 - \frac{1}{2(\tau_f - A)} \right] \rho (u_x a_{1y} + u_y a_{1x}) = 0, \end{aligned} \quad (\text{B17b})$$

$$\begin{aligned} \partial_{t_1}(\rho u_y) + \partial_{0x} \left[\left(1 - \frac{1}{2(\tau_f - A)} \right) m_{f8}^{(1)} \right] + \partial_{0y} \left[\frac{1}{6} \left(1 - \frac{1}{2(\tau_f - A)} \right) m_{f1}^{(1)} + \frac{1}{2} \left(1 - \frac{1}{2(\tau_f - A)} \right) m_{f7}^{(1)} \right] \\ + \frac{\delta_t}{2} \partial_{0x} \left[1 - \frac{1}{2(\tau_f - A)} \right] \rho (u_x a_{1y} + u_y a_{1x}) + \delta_t \partial_{0y} \left[1 - \frac{1}{2(\tau_f - A)} \right] \rho u_y a_{1y} = 0, \end{aligned} \quad (\text{B17c})$$

where Eq. (B15) has been used to derive Eq. (B17).

From the macroscopic equations in terms of ρ and $\rho\mathbf{u}$ in Eq. (B16), one can obtain the following expression under the assumption of low Mach number:

$$\partial_{t_0}(\rho u_\alpha u_\beta) = -u_\alpha \partial_{0\beta} p - u_\beta \partial_{0\alpha} p + \rho u_\alpha a_{1\beta} + \rho u_\beta a_{1\alpha}, \quad (\text{B18})$$

where $p = c_s^2 \rho = \frac{1}{3} \rho$. And then, we can derive the equations for $m_{f1}^{(1)}$, $m_{f7}^{(1)}$, and $m_{f8}^{(1)}$:

$$-\frac{1}{(\tau_f - A)\delta_t} m_{f1}^{(1)} = 2\rho(\partial_{0x}u_x + \partial_{0y}u_y) + 3\frac{1}{\tau_f - A} \rho \mathbf{a}_1 \cdot \mathbf{u}, \quad (\text{B19a})$$

$$-\frac{1}{(\tau_f - A)\delta_t} m_{f7}^{(1)} = \frac{2\rho}{3}(\partial_{0x}u_x - \partial_{0y}u_y) + \frac{1}{\tau_f - A} \rho(a_{1x}u_x - a_{1y}u_y), \quad (\text{B19b})$$

$$-\frac{1}{(\tau_f - A)\delta_t} m_{f8}^{(1)} = \frac{\rho}{3}(\partial_{0x}u_y + \partial_{0y}u_x) + \frac{1}{2(\tau_f - A)} \rho(a_{1x}u_y + a_{1y}u_x). \quad (\text{B19c})$$

Rewriting Eq. (B17) by the results of Eq. (B19) yields the hydrodynamic equations at the t_1 scale

$$\partial_{t_1}\rho = 0, \quad (\text{B20a})$$

$$\partial_{t_1}(\rho u_x) = \partial_{0x}[\rho\nu(\partial_{0x}u_x - \partial_{0y}u_y) + \rho\xi(\partial_{0x}u_x + \partial_{0y}u_y)] + \partial_{0y}[\rho\nu(\partial_{0x}u_y + \partial_{0y}u_x)], \quad (\text{B20b})$$

$$\partial_{t_1}(\rho u_y) = \partial_{0x}[\rho\nu(\partial_{0x}u_y + \partial_{0y}u_x)] + \partial_{0y}[\rho\nu(\partial_{0y}u_y - \partial_{0x}u_x) + \rho\xi(\partial_{0x}u_x + \partial_{0y}u_y)], \quad (\text{B20c})$$

where ν and ξ are the kinematic and bulk viscosities and given by

$$\nu = c_s^2(\tau_f - A - \frac{1}{2})\delta_t, \quad \xi = c_s^2(\tau_f - A - \frac{1}{2})\delta_t. \quad (\text{B21})$$

Coupling the equations at the t_0 and t_1 scales, i.e., Eqs. (B16) and (B20), the Navier-Stokes equations can be obtained:

$$\partial_t \rho + \nabla \cdot (\rho \mathbf{u}) = 0, \quad (\text{B22a})$$

$$\partial_t(\rho \mathbf{u}) + \nabla \cdot (\rho \mathbf{u} \mathbf{u}) = -\nabla p + \nabla \cdot \boldsymbol{\tau} + \rho \mathbf{a}, \quad (\text{B22b})$$

where $\boldsymbol{\tau}$ is the shear stress and defined by $\boldsymbol{\tau} = 2\rho\nu\overset{\circ}{\mathbf{S}} + \rho\xi(\nabla \cdot \mathbf{u})\mathbf{I}$, in which $\overset{\circ}{\mathbf{S}} = \mathbf{S} - [\frac{1}{D}\text{tr}(\mathbf{S})]\mathbf{I}$ and D is the dimension of the considered flow system. For incompressible flows, the shear stress is simplified to be $\boldsymbol{\tau} = 2\rho\nu\mathbf{S}$, and Eq. (B22) is reduced to Eq. (1).

2. Derivation of the CDE

From the explicit expression of Eq. (B13e), the following three equations at the t_0 timescale can be obtained:

$$\partial_{t_0}\phi + \partial_{0x}(\phi u_x) + \partial_{0y}(\phi u_y) = Q_1, \quad (\text{B23a})$$

$$\partial_{t_0}(\phi u_x) + \partial_{0x} \left[\phi \left(\frac{2}{3} + u_x^2 \right) \right] + \partial_{0y}(\phi u_x u_y) = -\frac{2}{(\tau_\phi - B + \frac{1}{2})\delta_t} m_{g3}^{(1)} + \left[1 - \frac{1}{\tau_\phi - B + \frac{1}{2}} \right] (\phi a_{1x} + Q_1 u_x), \quad (\text{B23b})$$

$$\partial_{t_0}(\phi u_y) + \partial_{0x}(\phi u_x u_y) + \partial_{0y} \left[\phi \left(\frac{2}{3} + u_y^2 \right) \right] = -\frac{2}{(\tau_\phi - B + \frac{1}{2})\delta_t} m_{g5}^{(1)} + \left[1 - \frac{1}{\tau_\phi - B + \frac{1}{2}} \right] (\phi a_{1y} + Q_1 u_y), \quad (\text{B23c})$$

where Eq. (B15) is adopted to derive Eq. (B23a). Similarly, the equation of conservative variable ϕ at the t_1 timescale can be extracted from Eq. (B14b):

$$\partial_{t_1}\phi + \partial_{0x}\left\{\left(1 - \frac{1}{\tau_\phi - B + \frac{1}{2}}\right)\left[m_{g_3}^{(1)} + \frac{\delta_t}{2}(\rho\phi a_{1x} + Q_1 u_x)\right]\right\} + \partial_{0y}\left\{\left(1 - \frac{1}{\tau_\phi - B + \frac{1}{2}}\right)\left[m_{g_5}^{(1)} + \frac{\delta_t}{2}(\rho\phi a_{1y} + Q_1 u_y)\right]\right\} = 0. \quad (\text{B24})$$

With the help of Eqs. (B16) and (B23a) at the t_0 timescale, we can deduce that

$$\partial_{t_0}(\phi u_\alpha) + \partial_{0\alpha}(\phi u_\alpha^2) + \partial_{0\beta}(\phi u_\alpha u_\beta) = u_\alpha Q_1 + \rho\phi a_{1\alpha}, \quad (\text{B25})$$

where $\nabla\rho/\rho = O(\text{Ma}^2)$ is adopted. Then, we can get the following expressions for $m_{g_3}^{(1)}$ and $m_{g_5}^{(1)}$ from Eqs. (B23b) and (B23c):

$$-\frac{2}{(\tau_\phi - B + \frac{1}{2})\delta_t}m_{g_3}^{(1)} = \frac{2}{3}\partial_{0x}\phi + \frac{1}{\tau_\phi - B + \frac{1}{2}}(\rho\phi a_{1x} + Q_1 u_x), \quad (\text{B26a})$$

$$-\frac{2}{(\tau_\phi - B + \frac{1}{2})\delta_t}m_{g_5}^{(1)} = \frac{2}{3}\partial_{0y}\phi + \frac{1}{\tau_\phi - B + \frac{1}{2}}(\rho\phi a_{1y} + Q_1 u_y). \quad (\text{B26b})$$

Substituting Eq. (B26) into Eq. (B24), it leads to

$$\partial_{t_1}\phi = \partial_{0x}\left[c_s^2\left(\tau_\phi - B - \frac{1}{2}\right)\delta_t\partial_{0x}\phi\right] + \partial_{0y}\left[c_s^2\left(\tau_\phi - B - \frac{1}{2}\right)\delta_t\partial_{0y}\phi\right]. \quad (\text{B27})$$

Combining (B23a) at the t_0 timescale and Eq. (B27) at the t_1 timescale, the final CDE are derived:

$$\partial_t\phi + \nabla \cdot (\mathbf{u}\phi) = \nabla \cdot (D\nabla\phi) + Q, \quad (\text{B28})$$

where the diffusion coefficient D is determined by $D = c_s^2(\tau_\phi - B - \frac{1}{2})\delta_t$.

3. Derivations of \mathbf{S} and $\nabla\phi$

Previous studies have reported that the shear rate \mathbf{S} and gradient term $\nabla\phi$ can be computed locally by the nonequilibrium part of the distribution function, as indicated in Eq. (15). Noteworthily, from the above multiscale analysis, the two gradient terms can also be calculated locally by the nonequilibrium part of some moment vectors while with second-order accuracy in space.

Multiplying ε on both sides of Eq. (B19) and assuming that $\varepsilon m_{fi}^{(1)} = m_{fi} - m_{fi}^{(\text{eq})} + O(\varepsilon^2)$, the local computation of \mathbf{S} can be obtained as follows:

$$\begin{aligned} \partial_x u_x + \partial_y u_y &= -\frac{m_1 - m_1^{(0)} + 3\delta_t \rho \mathbf{a} \cdot \mathbf{u}}{2\rho(\tau_f - A)\delta_t}, \\ \partial_x u_x - \partial_y u_y &= -\frac{3[m_7 - m_7^{(0)} + \delta_t \rho(a_x u_x - a_y u_y)]}{2\rho(\tau_f - A)\delta_t}, \\ \partial_x u_y + \partial_y u_x &= -\frac{3[m_8 - m_8^{(0)} + \frac{1}{2}\delta_t \rho(a_y u_x + a_x u_y)]}{\rho(\tau_f - A)\delta_t}. \end{aligned} \quad (\text{B29})$$

Similarly, multiplying Eq. (B26) by ε and following $\varepsilon m_{gi}^{(1)} = m_{gi} - m_{gi}^{(\text{eq})} + O(\varepsilon^2)$, we have

$$\begin{aligned} \partial_x \phi &= -\frac{3}{2\delta_t} \frac{2[q_3 - q_3^{(0)}] + \delta_t(\phi a_x + u_x Q)}{\tau_\phi - B + \frac{1}{2}}, \\ \partial_y \phi &= -\frac{3}{2\delta_t} \frac{2[q_5 - q_5^{(0)}] + \delta_t(\phi a_y + u_y Q)}{\tau_\phi - B + \frac{1}{2}}. \end{aligned} \quad (\text{B30})$$

[1] R. Benzi, S. Succi, and M. Vergassola, *Phys. Rep.* **222**, 145 (1992).
[2] S. Y. Chen and G. D. Doolen, *Annu. Rev. Fluid Mech.* **30**, 329 (1998).
[3] C. K. Aidun and J. R. Clausen, *Annu. Rev. Fluid Mech.* **42**, 439 (2010).

[4] X. M. Yu and B. C. Shi, *Appl. Math. Comput.* **181**, 958 (2006).
[5] G. W. Yan, *J. Comput. Phys.* **161**, 61 (2000).
[6] H. L. Lai and C. F. Ma, *Phys. Rev. E* **84**, 046708 (2011).
[7] P. L. Bhatnagar, E. P. Gross, and M. Krook, *Phys. Rev.* **94**, 511 (1954).
[8] P. Welander, *Ark. Fys.* **7**, 507 (1954).

- [9] I. Ginzburg, *Adv. Water Res.* **28**, 1171 (2005).
- [10] I. Ginzburg, F. Verhaeghe, and D. d’Humières, *Commun. Comput. Phys.* **3**, 427 (2008).
- [11] I. Ginzburg, F. Verhaeghe, and D. d’Humières, *Commun. Comput. Phys.* **3**, 519 (2008).
- [12] S. Ansumali, I. V. Karlin, and H. C. Öttinger, *Europhys. Lett.* **63**, 798 (2003).
- [13] S. Succi, I. V. Karlin, and H. Chen, *Rev. Mod. Phys.* **74**, 1203 (2002).
- [14] M. Geier, A. Greiner, and J. G. Korvink, *Phys. Rev. E* **73**, 066705 (2006).
- [15] M. Geier, M. Schönherr, A. Pasquali, and M. Krafczyk, *Comput. Math. Appl.* **70**, 507 (2015).
- [16] D. d’Humières, I. Ginzburg, M. Krafczyk, P. Lallemand, and L.-S. Luo, *Philos. Trans. R. Soc. London A* **360**, 437 (2002).
- [17] P. Lallemand and L.-S. Luo, *Phys. Rev. E* **61**, 6546 (2000).
- [18] P. Lallemand and L.-S. Luo, *Phys. Rev. E* **68**, 036706 (2003).
- [19] L.-S. Luo, W. Liao, X. W. Chen, Y. Peng, and W. Zhang, *Phys. Rev. E* **83**, 056710 (2011).
- [20] I. Rasin, S. Succi, and W. Miller, *J. Comput. Phys.* **206**, 453 (2005).
- [21] I. Ginzburg and P. M. Adler, *J. Phys. II (France)* **4**, 191 (1994).
- [22] R. Machado, *Front. Phys.* **9**, 490 (2014).
- [23] P. Prestininzi, A. Montessori, M. L. Rocca, and S. Succi, *Int. J. Mod. Phys. C* **27**, 1650037 (2016).
- [24] C. Pan, L.-S. Luo, and C. T. Miller, *Comput. Fluids* **35**, 898 (2006).
- [25] D. d’Humières, in *Rarefied Gas Dynamics: Theory and Simulations*, edited by B. D. Shizgal and D. P. Weave, Vol. 159 of Progress in Astronautics and Aeronautics (AIAA, Washington, DC, 1992), pp. 450–458.
- [26] T. Inamuro, *Philos. Trans. R. Soc. London A* **360**, 477 (2002).
- [27] T. Inamuro, *Fluid Dyn. Res.* **38**, 641 (2006).
- [28] T. Nishiyama, T. Inamuro, and S. Yasuda, *Comput. Fluids* **86**, 395 (2013).
- [29] M. Yoshino, Y. Hotta, T. Hirozane, and M. Endo, *J. Non-Newtonian Fluid Mech.* **147**, 69 (2007).
- [30] Y. Peng, C. Shu, Y. T. Chew, and T. Inamuro, *Phys. Rev. E* **69**, 016703 (2004).
- [31] L. Wang, J. C. Mi, X. H. Meng, and Z. L. Guo, *Commun. Comput. Phys.* **17**, 908 (2015).
- [32] X. G. Yang, B. C. Shi, and Z. H. Chai, *Phys. Rev. E* **90**, 013309 (2014).
- [33] X. H. Meng and Z. L. Guo, *Phys. Rev. E* **92**, 043305 (2015).
- [34] L. Wang, J. C. Mi, and Z. L. Guo, *Int. J. Heat Mass Tran.* **94**, 269 (2016).
- [35] Z. Wang, N. N. Dang, and J. Z. Zhang, *Int. J. Heat Mass Tran.* **108**, 691 (2017).
- [36] Q. Ma, Z. Q. Chen, and H. Liu, *Phys. Rev. E* **96**, 013313 (2017).
- [37] Y. Wang, C. Shu, L. M. Yang, and H. Z. Yuan, *J. Non-Newtonian Fluid Mech.* **235**, 20 (2016).
- [38] Y. Hu, D. C. Li, S. Shu, and X. D. Niu, *Int. J. Heat Mass Tran.* **104**, 544 (2017).
- [39] T. Krüger, H. Kusumaatmaja, A. Kuzmin, O. Shardt, G. Silva, and E. M. Viggien, in *The Lattice Boltzmann Method*, Graduate Texts in Physics (Springer, Cham, 2017), pp. 297–329.
- [40] W. F. Zhao, L. Wang, and W. A. Yong, *Physica A* **492**, 1570 (2018).
- [41] B. Chopard, J. L. Falcone, and J. Latt, *Eur. Phys. J. Special Topics* **171**, 245 (2009).
- [42] J. Latt and B. Chopard, *Math. Comput. Simul.* **72**, 165 (2006).
- [43] A. Montessori, G. Falcucci, P. Prestininzi, M. La Rocca, and S. Succi, *Phys. Rev. E* **89**, 053317 (2014).
- [44] Z. H. Chai and T. S. Zhao, *Phys. Rev. E* **87**, 063309 (2013); **90**, 013305 (2014).
- [45] Z. L. Guo, C. G. Zheng, and B. C. Shi, *Phys. Rev. E* **65**, 046308 (2002).
- [46] A. J. C. Ladd, *J. Fluid Mech.* **271**, 285 (1994).
- [47] B. Chun and A. J. C. Ladd, *Phys. Rev. E* **75**, 066705 (2007).
- [48] Z. L. Guo, C. G. Zheng, and B. C. Shi, *Phys. Fluids* **14**, 2007 (2002).
- [49] G. de Vahl Davis, *Int. J. Numer. Methods Fluids* **3**, 249 (1983).
- [50] M. Hortmann, M. Perić, and G. Scheuerer, *Int. J. Numer. Methods Fluids* **11**, 189 (1990).
- [51] Z. L. Guo, B. C. Shi, and C. G. Zheng, *Int. J. Numer. Meth. Fluids* **39**, 325 (2002).
- [52] Z. L. Guo and C. Shu, *Lattice Boltzmann Method and its Applications in Engineering* (World Scientific, Singapore, 2013).